Table 1
Reproductive organ weights in male ICR and C57BL/6N mice exposed to E_2

Dose (μg/kg/day)	No. males treated	Start of treatment (Administration period)	Age at termination	Final body weight (g)	Testes (g)	Epididymides (g)	Seminal vesicles (g)
ICR							
0	10	27 days old (21 days)	7 weeks old	38.52 ± 0.77[a]	0.221 ± 0.011[b] 0.577 ± 0.037[c]	0.074 ± 0.002 0.192 ± 0.007	0.288 ± 0.023 0.743 ± 0.051
10	10	27 days old (21 days)	7 weeks old	35.69 ± 0.78	0.203 ± 0.012 (92%)[d] 0.563 ± 0.034 (98%)	0.069 ± 0.003 (93%) 0.194 ± 0.007 (101%)	0.263 ± 0.015 (91%) 0.739 ± 0.042 (99%)
C57BL/6N							
0	10	27 days old (21 days)	7 weeks old	19.15 ± 0.45	0.130 ± 0.005 0.673 ± 0.024	0.042 ± 0.002 0.216 ± 0.008	0.100 ± 0.008 0.520 ± 0.030
10	10	27 days old (21 days)	7 weeks old	19.61 ± 0.34	0.108 ± 0.017* (83%) 0.548 ± 0.083* (81%)	0.028 ± 0.004** (67%) 0.141 ± 0.018** (65%)	0.057 ± 0.011** (57%) 0.284 ± 0.050** (55%)

[a]mean ± S.E.
[b]absolute weight.
[c]relative weight (organ weight/terminal body weight) × 100.
[d]percentage of control.
*Significantly different from the control, $P < 0.05$.
**Significantly different from the control, $P < 0.01$.

2, 20, or 200 μg/kg by oral gavage from gestational day 11 through 17. The administration period was determined according to the protocol of the study by Cagen et al. [8]. The dosages were determined on the basis of body weight on the day of treatment. Administration was performed at a defined time (12:00). Ten pregnant mice were given 0.5% carboxymethyl cellulose (5 ml/kg) as controls. Forty untreated female mice were allowed to give birth. All the BPA-treated and control dams were subjected to cesarean section on day 18 of gestation. The day of cesarean section was considered as postnatal day 0. The neonates obtained by cesarean section were fostered to untreated C57BL/6N females, one litter per female. On postnatal day 4, all female pups were discarded, and the number of males per litter was adjusted to 3 for each foster female. The males were weaned on postnatal day 21 and then individually housed in polycarbonate cages, where they were allowed to grow and sexually mature. At 12 weeks of age, all males were weighed. Five males per group were anesthetized and transcardiac perfusion was carried out. The remaining males (25 males per group) were subjected to necropsy. Subsequently, the testes, epididymides, and seminal vesicles with coagulating glands were weighed, and the left cauda epididymis of each male was homogenized to determine the sperm density. Finally, weighed organs were fixed in Bouin's solution for histologic evaluation.

Animal care and use conformed to published guidelines [15].

2.6. Analysis of data

Data were analyzed, where appropriate, to determine the statistical significance of differences between the control and E_2- or BPA-treated groups; $P < 0.05$ and $P < 0.01$ were taken to indicate statistical significance. Individual data or mean values of each litter were treated as single samples, and homogeneity of variance of these samples among groups was analyzed initially using Bartlett's test. When homogeneity of variance was confirmed, one-way analysis of variance was applied to detect significance of differences among groups. If a significant difference was detected among groups, Dunnett's test was applied for multiple comparisons. When variance was not homogeneous or there was any group in which the variance was zero, Kruskal-Wallis analysis of ranks was applied. If significance was detected among groups, Dunnett's test was applied for multiple comparisons.

3. Results

3.1. Susceptibility to E_2 between C57BL/6N and ICR mice

Table 1 shows the reproductive organ weights of C57BL/6N and ICR males treated s.c. with E_2 from postnatal days 27 to 48. There were no significantly different in the absolute or relative weights (testes, epididymides, and seminal vesicles) between the E_2-treated males and the controls in ICR strain. In marked contrast, significant decreases in the absolute and relative weights of reproductive organs were detected in the E_2-treated males of the C57BL/6N strain as compared with those of the controls. In particular, relative weight of seminal vesicles in the E_2-treated males of this strain was 55% that of the controls. At necropsy, three and five C57BL/6N males treated with E_2 showed marked atrophy of the testes and seminal vesicles, respectively, while no macroscopic changes of the reproductive organs were observed in the ICR males treated with

Table 2
Histopathologic findings in ICR and C57BL/6N male mice exposed to E_2

Strain	ICR																C57BL/6N											
Dose (μg/kg/day)	0							10									0							10				
Animal No.	1	2	3	4	5	6	7	1	2	3	4	5	6	7	8		1	2	3	4	5	6	7	1	2	3	4	5	6
Testis																													
Multinucleated giant cell, unilateral	–	–	–	–	–	–	–	–	–	–	–	–	–	–	–		–	–	–	–	–	–	–	±	–	–	–	–	–
Decrease in elongate spermatid, unilateral	–	–	–	–	–	–	–	–	–	–	–	–	–	–	–		–	–	–	–	–	–	–	±	–	–	–	+	–
Decrease in elongate spermatid, bilateral	–	–	–	–	–	–	–	–	–	–	–	–	–	–	–		–	–	–	–	–	–	–	–	–	–	–	–	++
Atrophy of Leydig cell, bilateral	–	–	–	–	–	–	–	–	–	–	–	–	–	–	–		–	–	–	–	–	–	–	±	–	–	±	+	++
Epididymis																													
Cell debris in lumen, unilateral	–	–	–	–	–	–	–	–	–	–	–	–	–	–	–		+	–	–	–	–	–	+	–	–	–	–	±	–
Cell debris in lumen, bilateral		–							–	–										+	+	–							+
Decrease in sperm, unilateral	–	–	–	–	–	–	–	–	–	–	–	–	–	–	–		+	–	–	–	–	–	+	–	–	–	–	–	–
Decrease in sperm, bilateral	–	–	–	–	–	–	–	–	–	–	–	–	–	–	–		–	–	–	+	+	–	–	–	–	–	–	+	+++
Seminal vesicle																													
Atrophy	–	–	–	–	–	–	–	–	–	–	–	–	–	–	–		–	–	–	–	–	–	–	+	–	–	–	++	+++

–, Negative; ±, Very slight; +, Slight; ++, Moderate; +++, Severe.

E_2. Histopathologic findings of the reproductive organs in ICR and C57BL/6N mice treated with E_2 are shown in Table 2, and the representative changes observed in C57BL/6N mice are shown in Fig. 1. Only a few elongate spermatids were observed in seminiferous tubules of C57BL/6N mice treated with E_2. The number of size of Leydig cells of C57BL/6N mice treated with E_2 was decreased as compared with the controls. In addition, no sperm were observed in the lumen of the epididymal ducts, and the lumen of the seminal vesicles contained no secretions. Three other C57BL/6N males treated with E_2 showed similar but slight changes in the testis, epididymis, and seminal vesicles. C57BL/6N males in the control group showed no abnormalities except for cell debris and a slight decrease in sperm in the epididymal duct. In ICR males treated with E_2, no histopathologic changes in the reproductive organs were observed.

3.2. Low-dose effects of BPA in C57BL/6N male mice

No adult or immature C57BL/6N male mice exposed to BPA for 6 days or 3 weeks, respectively, died during the study period. In addition, there were no significant differences in body weight gain from the day of commencement of administration to the day of necropsy between the BPA-treated groups and the controls. No significant differences were found in embryo mortality or viability after birth between the BPA-treated groups and the control, nor in the body weight gain until necropsy (data not shown).

Table 3 shows the percentages of control values for the reproductive organ weights in C57BL/6N males exposed to BPA at various stages. In males exposed to BPA at the mature or immature stage after weaning there were no significant differences between the BPA-treated groups and the controls in terminal body weight or reproductive organ weights (testes, epididymides, seminal vesicles), or their relative weights.

In C57BL/6N males exposed to BPA as embryos at the organogenic stage, a significant decrease in the absolute weight of seminal vesicles in the 2 μg/kg group was found as compared with the controls, but the effect was not dose-dependent, suggesting that the decrease in the weight of the seminal vesicles was not related to BPA administration.

Fig. 2 shows the numbers of sperm per gram cauda epididymis of C57BL/6N males exposed to BPA at various stages. There were no significant differences in the density of sperm between the BPA-treated groups and the controls.

With regard to the histopathologic observations of the testes, epididymides, seminal vesicles, and prostate by light and electron microscopy, slight atrophy of the seminiferous tubules and multinucleated giant cells in immature seminiferous tubules were observed in males exposed to BPA after weaning for 3 weeks in all of the BPA-treated groups and the controls. In one of 30 males exposed to BPA at 2 μg/kg after weaning for 3 weeks, diffuse atrophy of the seminiferous tubules was found. In C57BL/6N males exposed to BPA at the mature stage or embryonic stage, no histopathologic changes that may have resulted in a decreased number of germ cells including mature sperm were observed in any parts of the reproductive tract.

4. Discussion

Significant decreases in weights of reproductive organs were detected in C57BL/6N male mice treated with E_2 from postnatal day 27 to 48 as compared with those of the controls. In particular, relative weight of seminal vesicles in the E_2-treated males of the C57BL/6N was 55% of that of the controls. Male C57BL/6N mice treated with E_2 showed

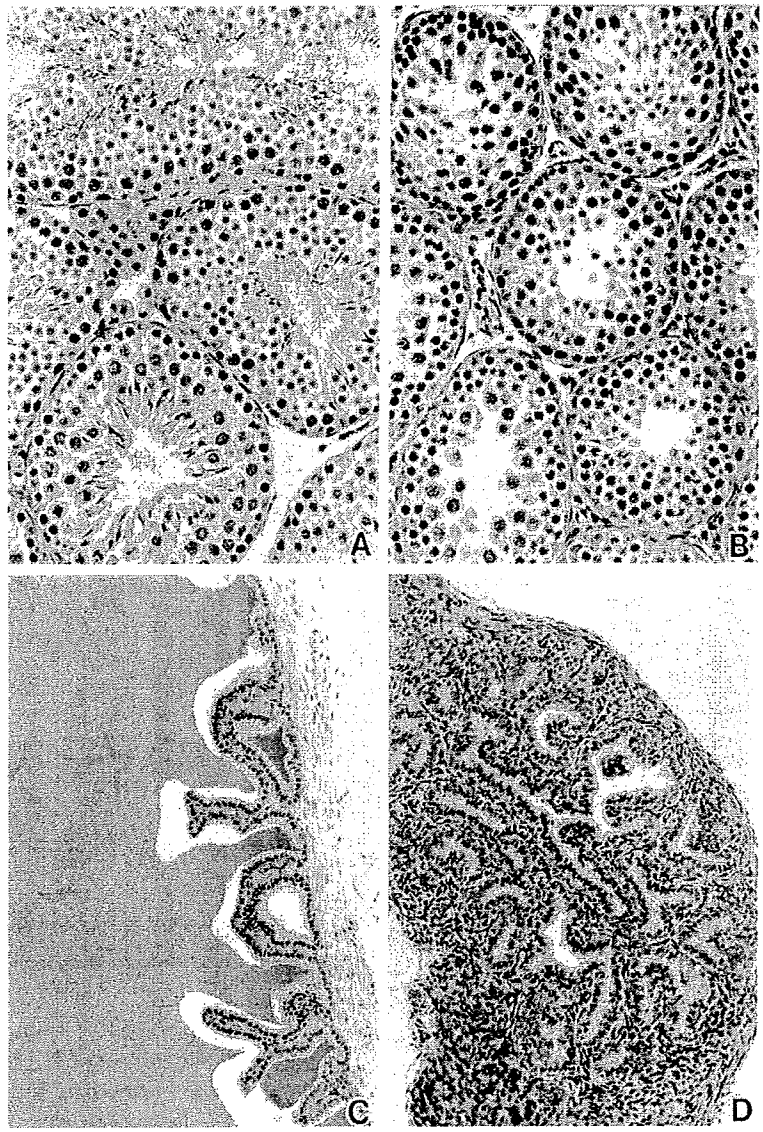

Fig. 1. Histopathologic changes in C57BL/6N male mice exposed s.c. to E_2 from postnatal day 27 to 48. (A) Control male testis. No abnormalities were observed. H&E, ×350. (B) Testis from BPA-treated male. Only a few elongate spermatids were observed in the seminiferous tubules.The number and size of Leydig cells was decreased. H&E, ×350. (C) Control seminal vesicle. No abnormalities were observed. H&E, ×175. (D) Seminal vesicle from BPA-treated male. The lumen contained no secretions. H&E, ×175.

marked atrophy of the testes and seminal vesicle as well as histopathologic changes of the reproductive organs (see Table 2). In contrast, no macroscopic or microscopic changes of the reproductive organs were detected in males of ICR mice treated with E_2. Taken together, these observations suggested that male C57BL/6N mice are extremely sensitive to the effects of E_2 similar to the male C57BL/6J mice reported previously [13], while male ICR mice are extremely resistant to E_2.

In the present study, reproductive organ weights (testes, epididymides, seminal vesicles) in C57BL/6N males exposed to BPA at the mature or immature stage did not differ from those of controls. Ohsako et al. [14] reported that testes weight and daily sperm production of Sprague-Dawley rats 36 days after the first treatment with BPA at 20 μg/kg/day for 6 days were significantly decreased, and concluded that even at very low doses BPA affected spermatogenesis of mature rats. These results were incompatible with those of the present study. There were no significant differences in the density of sperm between the groups exposed to BPA at various stages and the controls. In addition, the numbers of sperm in the BPA-treated and control groups were within the range of the other control data based on information gathered in reproductive and developmental toxicity studies using C57BL/6N mice in our laboratory over a period of 3 years, suggesting that exposure of mice to low-dose BPA at various stages did not affect sperm production.

Table 3
Reproductive organ weights in male C57BL/6N mice exposed to BPA at various stages

Dose (μg/kg/day)	No. mice treated	Start of treatment (Administration period)	Age at termination	No. males/ No. litters	Final body weight (g)	Testes (g)	Epididymides (g)	Seminal vesicles (g)
0	20 males	12 weeks old (6 days)	17 weeks old	15	29.77 ± 0.59[a]	0.150 ± 0.008[b]	0.071 ± 0.003	0.419 ± 0.016
						0.502 ± 0.042[c]	0.237 ± 0.015	1.395 ± 0.033
2	20 males	12 weeks old (6 days)	17 weeks old	15	29.00 ± 0.47	0.157 ± 0.001	0.072 ± 0.001	0.417 ± 0.030
						0.536 ± 0.013	0.246 ± 0.006	1.431 ± 0.128
20	20 males	12 weeks old (6 days)	17 weeks old	15	29.81 ± 0.77	0.159 ± 0.005	0.078 ± 0.003	0.407 ± 0.008
						0.539 ± 0.026	0.262 ± 0.013	1.366 ± 0.050
200	20 males	12 weeks old (6 days)	17 weeks old	15	29.75 ± 0.75	0.159 ± 0.004	0.072 ± 0.001	0.411 ± 0.020
						0.545 ± 0.017	0.246 ± 0.011	1.382 ± 0.083
0	30 males	21 days old (21 days)	6 weeks old	25/10	17.15 ± 0.29	0.119 ± 0.002	0.031 ± 0.001	0.045 ± 0.003
						0.713 ± 0.014	0.181 ± 0.006	0.259 ± 0.015
2	30 males	21 days old (21 days)	6 weeks old	25/10	18.22 ± 0.67	0.117 ± 0.017	0.033 ± 0.003	0.044 ± 0.006
						0.663 ± 0.084	0.187 ± 0.013	0.247 ± 0.028
20	30 males	21 days old (21 days)	6 weeks old	25/10	16.08 ± 0.83	0.116 ± 0.012	0.030 ± 0.003	0.043 ± 0.008
						0.701 ± 0.056	0.184 ± 0.011	0.253 ± 0.041
200	30 males	21 days old (21 days)	6 weeks old	25/10	16.83 ± 0.34	0.115 ± 0.006	0.030 ± 0.001	0.045 ± 0.003
						0.677 ± 0.038	0.173 ± 0.007	0.263 ± 0.014
0	10 dams	Gestational day 11 (7 days)	12 weeks old	25/10	24.70 ± 0.28	0.149 ± 0.003	0.060 ± 0.001	0.248 ± 0.006
						0.617 ± 0.014	0.249 ± 0.004	1.028 ± 0.027
2	10 dams	Gestational day 11 (7 days)	12 weeks old	25/10	23.99 ± 0.50	0.146 ± 0.003	0.058 ± 0.002	0.234 ± 0.003*
						0.612 ± 0.012	0.242 ± 0.006	0.968 ± 0.038
20	10 dams	Gestational day 11 (7 days)	12 weeks old	25/10	23.85 ± 0.25	0.142 ± 0.002	0.057 ± 0.002	0.243 ± 0.011
						0.594 ± 0.009	0.239 ± 0.007	1.009 ± 0.047
200	10 dams	Gestational day 11 (7 days)	12 weeks old	25/10	24.75 ± 0.52	0.149 ± 0.003	0.060 ± 0.001	0.250 ± 0.008
						0.608 ± 0.012	0.240 ± 0.005	1.008 ± 0.022

[a]mean ± S.E.
[b]absolute weight.
[c]relative weight: (organ weight/terminal body weight) × 100.
*Significantly different from the control, $P < 0.05$.
Five males in each group were anesthetized and transcardiac perfusion was performed for histologic observance testes, epididymides, seminal vesicles, and prostates with an electron microscope.

Developmental and reproductive toxicity of high doses of BPA have been demonstrated in rats and mice. Persistent estrus was observed in ovariectomized rats injected twice/day for 3 consecutive days with 100 mg BPA [16]. Intraperitoneal (i.p.) injection of BPA at 125 mg/kg on gestational day 1 through 15 also interfered with the maintenance of pregnancy and reduced the number of live fetuses per litter in Sprague-Dawley rats [17]. However, no significant developmental toxicity of BPA was observed in CD rats or CD-1 mice exposed to BPA (rats, 640 mg/kg: mice 1000 mg/kg) by gavage from gestational day 6 through 15 [18]. In addition, neonatal exposure to BPA at 300 mg/kg did not produce detectable effects on the volume of the sexually dimorphic nucleus of the preoptic area (SDN-POA), nor in development of male reproductive organs or reproductive function after puberty in Sprague-Dawley rats [19]. Oral administration of BPA at much lower doses has also been reported to affect male reproductive organ parameters such as the prostate gland (increase in fresh tissue weight at 2 or 20 μg/kg/day), preputial glands (increase in tissue weight at 2 μg/kg/day), and epididymis (decrease in tissue weight at 2 μg/kg/day), and the efficiency of sperm production (decrease in daily sperm production per g testis at 20 μg/kg/day) in CF-1 mice exposed to BPA during prenatal development from GD 11 to GD 17 [5,6]. However, the low-dose effects of BPA have been controversial. Other groups reported no treatment-related effects of BPA at the same and additional low-dose levels given at the same time during pregnancy to CF-1 mice [7,8]. In the experiments in Sprague-Dawley rats, Welsch et al. [12] demonstrated the lack of effects of perinatal exposure to low doses of BPA on ventral prostate weight of male offspring. Elswick et al. [9] also reported that rats exposed to low doses of BPA during the perinatal period did not display significant differences in hormone levels, sperm counts, or immunohistochemical ventral prostate androgen receptor (AR) levels. Recently, two- or three-generation reproductive toxicity studies of BPA administered by gastric intubation or in the diet were performed. The results of these multigeneration studies indicated that low doses of BPA between 0.2 and 200 μg/kg or between 0.015 and 75 ppm over 2 or 3 generations did not cause significant compound-related changes in reproductive or developmental parameters in rats [10,20]. At present, we cannot explain the differences between the results of the present study and those of vom Saal [6] and others [5] and the rat study of Ohsako et al. [14]. These

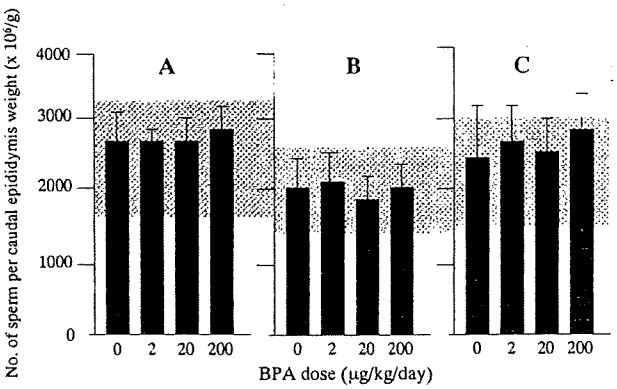

Fig. 2. Numbers of sperm per gram cauda epididymis of male C57BL/6N mice exposed to low-dose BPA at various developmental stages; (A) sexually mature, (B) juvenile, or (C) embryonic/fetal stage. The shadowed regions represent the range of sperm number per gram cauda epididymis in the historical controls in C57BL/6N male mice (left, 17–18 weeks old; middle; 6 weeks old; right, 12–13 weeks old).

discrepancies make the assessment of xenoestrogenic compounds extremely controversial, while concomitantly highlighting the need to resolve these potential important public health concerns [21]. Ashby suggested that some of the failures to repeat observations are probably associated with the many subtle differences that exist between formally identical studies conducted in different laboratories (radio playing quietly in the animal room, soy content of the animal diet, average body weight of the control CF-1 mice, genetic drift of CF-1 mice) [7]. Some chemicals produce small changes in sex-related biologic endpoints that may be difficult to reproduce among laboratories.

Diffuse atrophy of the seminiferous tubules was observed in one C57BL/6N male mouse exposed to BPA at 2 μg/kg after weaning for 3 weeks in the present study. As this was the only case in which an abnormality was found in the testes from males exposed to BPA at various stages, it was not clear whether this change had arisen spontaneously or as a consequence of BPA exposure. In C57BL/6N males exposed to BPA at the mature stage or embryonic stage, no microscopic changes that may have resulted in the decreased number of germ cells including mature sperm were observed in any parts of the reproductive tract. These histopathologic findings were consistent with the lack of effects on sperm density following BPA administration.

When assessing the biologic activity of putative estrogenic compounds in animal model systems, it is important to consider species and strain differences. Strain differences in response to estrogenic stimuli have been demonstrated previously. Gorski and coworkers [22–24] found that the potent estrogens diethylstilbestrol and E_2 induce an overgrowth of lactotropes in the pituitary glands of F344 rats but not in those of outbred strains of rats. Spearow et al. [13] found marked strain-related differences in the susceptibility of mice to estradiol-induced disruption of testicular development. Estradiol treatment during juvenile development resulted in the suppression of testis weight in mouse strains CD-1, C57BL/6J, C17/Jls, S15/Jls, E/Jls and CN-/Jls [13]. Among these, C57BL/6J mice were extremely sensitive with the lowest E_2 dose used (2.5 μg) producing 60% suppression of testis weight in this strain. Unlike C57BL/6J mice in which low to moderate doses of E_2 completely blocked spermatogenesis, CD-1 mice showed very little inhibition of spermatogenesis in response to increasing doses of E_2. Other studies have shown differences in the efficacy of E_2 in stimulation of uterine DNA synthesis between strains of mice [25,26]. In our preliminary study, female ICR and C57BL/6N mice were exposed to various estrogens and endocrine disrupting chemicals during pregnancy, and C57BL/6N embryos were more sensitive (10- to 100-fold) to the lethal effects and disruptive effects of all of these chemicals on development of the reproductive organs than ICR embryos (Nagao, unpublished data).

5. Concluding remarks

In the present study, C57BL/6N mice that are highly susceptible to endocrine disruption by estrogen were used to evaluate the effects of low-dose BPA following exposure at various stages. Based on the results of the present study and the considerable body of literature on the effects of BPA at similar and much higher doses, low-dose BPA should not be considered as a testicular toxicant.

References

[1] Olea N, Pulgar R, Perez P, Olea-Serrano F, Rivas A, Novillo-Fertrell A, Pedraza V, Soto AM, Sonnenschein C. Estrogenicity of resin-based composites and sealants used in dentistry. Environ Health Perspect 1996;104:298–305.

[2] Krishnan AV, Stathis P, Permuth SF, Tokes L, Feldman D. Bisphenol-A: an estrogenic substance is released from polycarbonate flasks during autoclaving. Endocrinology 1993;132:2279–86.

[3] Gaido KW, Leonard LS, Lovell S, Gould JC, Babai D, Portier CJ, McDonnell DP. Evaluation of chemicals with endocrine modulating activity in a yeast-based steroid hormone receptor gene transcription assay. Toxicol Appl Pharmacol 1997;143:205–12.

[4] Kuiper GG, Lemmen JG, Carlsson B, Corton JC, Safe SH, van der Saag PT, van der Burg B, Gustafsson JA. Interaction of estrogenic chemicals and phytoestrogens with estrogen receptor beta. Endocrinology 1998;139:4252–63.

[5] Nagel SC, vom Saal FS, Thayer KA, Dhar MG, Boechler M, Welshons WV. Relative binding affinity-serum modified access (RBA-SMA) assay predicts the relative in vivo bioactivity of the xenoestrogens bisphenol A and octylphenol. Environ Health Perspect 1997; 105:70–6.

[6] vom Saal FS, Cooke PS, Buchanan DL, Palanza P, Thayer KA, Nagel SC, Parmigiani S, Welshons WV. A physiologically based approach to the study of bisphenol A and other estrogenic chemicals on the size of reproductive organs, daily sperm production, and behavior. Toxicol Ind Health 1998;14:239–60.

[7] Ashby J, Tinwell H, Haseman J. Lack of effects for low dose levels of bisphenol A and diethylstilbestrol on the prostate gland of CF1 mice exposed in utero. Regul Toxicol Pharmacol 1999;30:156–66.

[8] Cagen SZ, Waechter JM, Dimond SS, Breslin WJ, Butala JH, Jekat FW, Joiner RL, Shiotsuka RN, Veenstra GE, Harris LR. Normal reproductive organ development in CF-1 mice following prenatal exposure to bisphenol A. Toxicol Sci 1999;50:36–44.
[9] Elswick BA, Janszen DB, Gould JC, Stedman DB, Welsch F. Effects of perinatal exposure to low doses of bisphenol A in male offspring of Sprague-Dawley rats. Toxicol Sci 2000;54(Suppl.):256A.
[10] Ema M, Fujii S, Furukawa M, Kiguchi M, Ikka T, Harazono A. Rat two-generation reproductive toxicity study of bisphenol A. Reprod Toxicol 2001;15:505–23.
[11] Tyl RW, Myers CB, Marr MC, Chang TY, Seely JC, Brine DR, Veselica MM, Fail PA, Joiner RL, Butala JH, Dimond SS, Shiotsuka RN, Stropp G, Veenstra GE, Waechter JM, Harris LR. Three-generation reproductive toxicity study of bisphenol A (BPA) administered in the diet to CD® (Sprague-Dawley) rats. Reprod Toxicol 2001;15:596.
[12] Welsch F, Elswick BA, Janszen DB, Robinette CL. Lack of effects of perinatal exposure to low doses of bisphenol A on male rat offspring ventral prostate glands. Reprod Toxicol 2001;15:597.
[13] Spearow JL, Doemeny P, Sera R, Leffler R, Barkley M. Genetic variation in susceptibility to endocrine disruption by estrogen in mice. Science 1999;285:1259–61.
[14] Ohsako S, Sakaue M, Ishimura R, Kurosawa S, Yonemoto J, Tohyama C. Effects of low-dose bisphenol-A on rat spermatogenesis. International Symposium on Environmental Endocrine Disruptor's 99. Abstract: 107 (Japanese).
[15] Guide for the Care and Use of Laboratory Animals. NIH Publication 86–23. Bethesda, MD: National Institute of Health, 1985.
[16] Dodds EC, Lawson W. Synthetic oestrogenic agents without the phenanthrene nucleus. Nature 1936;137:996.
[17] Hardin BD, Bond GP, Sikov MR, Andrew FD, Beliles RP, Niemeier RW. Testing of selected workplace chemicals for teratogenic potential. Scand J Work Environ Health 1981;7:66–75.
[18] Morrissey RE, George JD, Price CJ, Tyl RW, Marr MC, Kimmel CA. The developmental toxicity of bisphenol A in rats and mice. Fundam Appl Toxicol 1987;8:571–82.
[19] Nagao T, Saito Y, Usumi K, Kuwagata M, Imai K. Reproductive function in rats exposed neonatally to bisphenol A and estradiol benzoate. Reprod Toxicol 1999;13:303–11.
[20] Kwon S, Stedman DB, Elswick BA, Cattley RC, Welsch F. Pubertal development and reproductive functions of Crl:CD BR Sprague-Dawley rats exposed to bisphenol A during prenatal and postnatal development. Toxicol Sci 2000;55:399–406.
[21] Ashby J, Elliott BM. Editorial. Reproducibility of endocrine disruption data. Regul Toxicol Pharmacol 1997;26:94–5.
[22] Wiklund J, Wertz N, Gorski J. A comparison of estrogen effects on uterine and pituitary growth and prolactin synthesis in F344 and Holtzman rats. Endocrinology 1981;109:1700–7.
[23] Wiklund J, Gorski J. Genetic differences in estrogen-induced deoxyribonucleic acid synthesis in the rat pituitary: correlations with pituitary tumor susceptibility. Endocrinology 1982;111:1140–9.
[24] Wendell DL, Gorski J. Quantitative trait loci for estrogen-dependent pituitary tumor growth in the rat. Mamm Genome 1997;8:823–9.
[25] Lee AE. Cell division and DNA synthesis in the mouse uterus during continuous oestrogen treatment. J Endocrinol 1972;55:507–13.
[26] Martin L. Estrogens, anti-estrogens and the regulation of cell proliferation in the female reproductive tract in vivo. In: McLachlan JA, editor. Estrogens in the environment. New York: Elsevier, 1980. p. 103–29.

Differential contributions of Mesp1 and Mesp2 to the epithelialization and rostro-caudal patterning of somites

Yu Takahashi[1,*], Satoshi Kitajima[1], Tohru Inoue[1], Jun Kanno[1] and Yumiko Saga[2,*]

[1]Cellular & Molecular Toxicology Division, National Institute of Health Sciences, 1-18-1 Kamiyoga, Setagayaku, Tokyo 158-8501, Japan
[2]Division of Mammalian Development, National Institute of Genetics, Yata 1111, Mishima 411-8540, Japan
*Authors for correspondence (e-mail: yutak@nihs.go.jp and ysaga@lab.nig.ac.jp)

Accepted 29 November 2004

Development 132, 787-796
Published by The Company of Biologists 2005
doi:10.1242/dev.01597

Summary

Mesp1 and Mesp2 are homologous basic helix-loop-helix (bHLH) transcription factors that are co-expressed in the anterior presomitic mesoderm (PSM) just prior to somite formation. Analysis of possible functional redundancy of Mesp1 and Mesp2 has been prevented by the early developmental arrest of Mesp1/Mesp2 double-null embryos. Here we performed chimera analysis, using either Mesp2-null cells or Mesp1/Mesp2 double-null cells, to clarify (1) possible functional redundancy and the relative contributions of both Mesp1 and Mesp2 to somitogenesis and (2) the level of cell autonomy of Mesp functions for several aspects of somitogenesis. Both Mesp2-null and Mesp1/Mesp2 double-null cells failed to form initial segment borders or to acquire rostral properties, confirming that the contribution of Mesp1 is minor during these events. By contrast, Mesp1/Mesp2 double-null cells contributed to neither epithelial somite nor dermomyotome formation, whereas Mesp2-null cells partially contributed to incomplete somites and the dermomyotome. This indicates that Mesp1 has a significant role in the epithelialization of somitic mesoderm. We found that the roles of the Mesp genes in epithelialization and in the establishment of rostral properties are cell autonomous. However, we also show that epithelial somite formation, with normal rostro-caudal patterning, by wild-type cells was severely disrupted by the presence of Mesp mutant cells, demonstrating non-cell autonomous effects and supporting our previous hypothesis that Mesp2 is responsible for the rostro-caudal patterning process itself in the anterior PSM, via cellular interaction.

Key words: Somitogenesis, Epithelial-mesenchymal conversion, Mesp2, Chimera analysis, Mouse

Introduction

Somitogenesis is not only an attractive example of metameric pattern formation but is also a good model system for the study of morphogenesis, particularly epithelial-mesenchymal interconversion in vertebrate embryos (Gossler and Hrabe de Angelis, 1997; Pourquié, 2001). The primitive streak, or tailbud mesenchyme, supplies the unsegmented paraxial mesoderm, known as presomitic mesoderm (PSM). Mesenchymal cells in the PSM undergo mesenchymal-epithelial conversion to form epithelial somites in a spatially and temporally coordinated manner. Somites then differentiate, in accordance with environmental cues from the surrounding tissues, into dorsal epithelial dermomyotome and ventral mesenchymal sclerotome (Borycki and Emerson, 2000; Fan and Tessier Lavigne, 1994). Hence, the series of events that occur during somitogenesis provide a valuable example of epithelial-mesenchymal conversion. The dermomyotome gives rise to both dermis and skeletal muscle, whereas the sclerotome forms cartilage and bone in both the vertebrae and the ribs. Each somite is subdivided into two compartments, the rostral (anterior) and caudal (posterior) halves. This rostro-caudal polarity appears to be established just prior to somite formation (Saga and Takeda, 2001).

Mesp1 and Mesp2 are closely related members of the basic helix-loop-helix (bHLH) family of transcription factors but share significant sequence homology only in their bHLH regions (Saga et al., 1996; Saga et al., 1997). During development of the mouse embryo, both *Mesp1* and *Mesp2* are specifically expressed in the early mesoderm just after gastrulation and in the paraxial mesoderm during somitogenesis. Mesp1/Mesp2 double-null embryos show defects in early mesodermal migration and thus fail to form most of the embryonic mesoderm, leading to developmental arrest (Kitajima et al., 2000). Mesp1-null embryos exhibit defects in single heart tube formation, due to a delay in mesodermal migration, but survive to the somitogenesis stage (Saga et al., 1999), suggesting that there is some functional redundancy, i.e. compensatory functions of Mesp2 in early mesoderm. During somitogenesis, both *Mesp1* and *Mesp2* are expressed in the anterior PSM just prior to somite formation. Although we have shown that Mesp2, but not Mesp1, is essential for somite formation and the rostro-caudal patterning of somites (Saga et al., 1997), a possible functional redundancy between Mesp1 and Mesp2 has not yet been clearly established.

To further clarify the contributions of Mesp1 and Mesp2 to somitogenesis, analysis of Mesp1/Mesp2 double-null embryos

is necessary, but because of the early mesodermal defects already described, these knockout embryos lack a paraxial mesoderm, which prevents any analysis of somitogenesis. We therefore adopted a strategy that utilized chimera analysis. As we have reported previously, the early embryonic lethality of a Mesp1/Mesp2 double knockout is rescued by the presence of wild-type cells in a chimeric embryo, but the double-null cells cannot contribute to the cardiac mesoderm (Kitajima et al., 2000). This analysis, however, focused only on early heart morphogenesis and did not investigate the behavior of Mesp1/Mesp2 double-null cells in somitogenesis. In this report, we focus upon somitogenesis and compare two types of chimeras using either Mesp1/Mesp2 double-null cells or Mesp2-null cells to investigate Mesp1 function during somitogenesis.

Another purpose of our chimera experiments was to elucidate the cell autonomy of Mesp functions. In the process of somite formation, mesenchymal cells in the PSM initially undergo epithelialization at the future segment boundary, independently of the already epithelialized dorsal or ventral margin of the PSM (Sato et al., 2002). Epithelial somite formation is disrupted in the Mesp2-null embryo, indicating that Mesp2 is required for epithelialization at the segment boundary. Although Mesp products are nuclear transcription factors and their primary functions must therefore be cell autonomous (transcriptional control of target genes), it is possible that the roles of Mesp2 in epithelialization are mediated by the non-cell autonomous effects of target genes. We therefore asked whether the defects in Mesp2-null cells during epithelialization could be rescued by the presence of surrounding wild-type cells. Additionally, we would expect to find that the role of Mesp2 in establishing rostro-caudal polarity is rescued in a similar way.

Our analysis suggests that Mesp1 and Mesp2 have redundant functions and are both cell-autonomously involved in the epithelialization of somitic mesoderm. In addition, our results highlight some non-cell autonomous effect of Mesp2-null and Mesp1/Mesp2-null cells.

Materials and methods

Generation of chimeric embryos

As described previously (Kitajima et al., 2000), chimeric embryos were generated by aggregating 8-cell embryos of wild-type mice (ICR) with those of mutant mice that were genetically marked with the *ROSA26* transgene (Zambrowicz et al., 1997). Mesp1/Mesp2 double-null embryos were generated by crossing *wko-del (+/–)* and *Mesp1(+/–)/Mesp2(+/cre)* mice as described previously (Kitajima et al., 2000). This strategy enables us to distinguish chimeric embryos derived from homozygous embryos, which have two different mutant alleles, from those derived from heterozygous embryos. Likewise, Mesp2-null embryos were generated by crossing *P2v1(+/–)* mice (Saga et al., 1997) and *P2GFP (+/gfp)* mice (Y.S. and S.K., unpublished) that were also labeled with the *ROSA26* locus. The genotype of the chimeric embryos was determined by PCR using yolk sac DNA.

Histology, histochemistry and gene expression analysis

The chimeric embryos were fixed at 11 days postcoitum (dpc) and stained in X-gal solution for the detection of β-galactosidase activity, as described previously (Saga et al., 1999). For histology, samples stained by X-gal were postfixed with 4% paraformaldehyde, dehydrated in an ethanol series, embedded in plastic resin (Technovit 8100, Heraeus Kulzer) and sectioned at 3 μm. The methods used for gene expression analysis by in-situ hybridization of whole-mount samples and frozen sections and skeletal preparation by Alcian Blue/Alizarin Red staining were described previously (Saga et al., 1997; Takahashi et al., 2000). Probes for in-situ hybridization for *Uncx4.1* (Mansouri et al., 1997; Neidhardt et al., 1997), *Delta-like 1 (Dll1)* (Bettenhausen et al., 1995) and *Paraxis* (Burgess et al., 1995) were kindly provided by Drs Peter Gruss, Achim Gossler and Alan Rawls, respectively. A probe for *EphA4* (Nieto et al., 1992) was cloned by PCR. For detection of actin filaments, frozen sections were stained with AlexaFluor 488-conjugated phalloidin (Molecular Probes) according to the manufacturer's protocol.

Results

Possible functional redundancy and different contributions of Mesp1 and Mesp2 in somitogenesis

During somitogenesis, both *Mesp1* and *Mesp2* are expressed in the anterior PSM just prior to somite formation and their expression domains overlap (Fig. 1A). Mesp1-null embryos form morphologically normal somites and show normal rostro-caudal patterning within each somite (Fig. 1B,E-H), indicating that Mesp1 is not essential for somitogenesis. By contrast, Mesp2 is essential for both the formation and rostro-caudal patterning of somites, as Mesp2-null embryos have no epithelial somites and lose rostral half properties, resulting in caudalization of the entire somitic mesoderm (Saga et al., 1997) (Fig. 1C,D).

Although somite formation and rostro-caudal patterning is disrupted in the Mesp2-null embryo, histological differentiation into dermomyotome and sclerotome is not affected. It is noteworthy that the Mesp2-null embryo still forms disorganized dermomyotomes without forming epithelial somites (Saga et al., 1997). As *Mesp1* is expressed at normal levels in the PSM of Mesp2-null embryos (Fig. 1C,D), it is possible that Mesp1 functions to rescue some aspects of somitogenesis in the Mesp2-null embryo. In order to further clarify the contributions of both Mesp1 and Mesp2 during somitogenesis, we therefore generated chimeric embryos with either Mesp2-null cells or Mesp1/Mesp2 double-null cells and compared the behavior of mutant cells during somitogenesis (Fig. 2).

Mesp2-null cells tend to be eliminated from the epithelial somite and the dermomyotome, but can partially contribute to both of these structures

We first generated Mesp2-null chimeric embryos (*Mesp2*$^{-/-}$ with *Rosa26*: wild) to analyze cell autonomy of Mesp2 function during somitogenesis. The control chimeric embryo (*Mesp2*$^{+/-}$ with *Rosa26*: wild) showed normal somitogenesis and a random distribution of X-gal stained cells (Fig. 3A). The Mesp2-null chimeric embryos formed abnormal somites that exhibited incomplete segmentation (Fig. 3B), but histological differentiation of dermomyotome and sclerotome was observed. Within the incomplete somite, X-gal-stained Mesp2-null cells were mainly localized in the rostral and central regions, surrounded by wild-type cells at the dorsal, ventral and caudal sides (Fig. 3B). The surrounding wild-type cells, however, did not form an integrated epithelial sheet, but consisted of several epithelial cell clusters. Such trends were more obviously observed in other sections, where wild-type cells were found to form multiple small epithelial clusters (Fig.

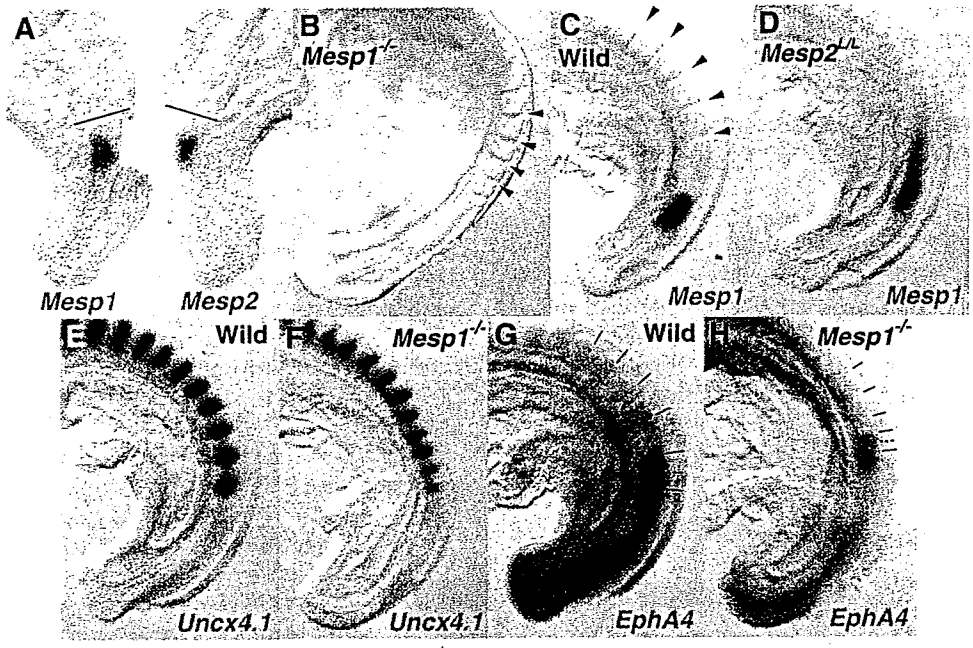

Fig. 1. *Mesp1* and *Mesp2* are co-expressed in the anterior PSM but have differing roles in somitogenesis. (A) Overlapping expression of *Mesp1* and *Mesp2* is revealed by in-situ hybridization using the left and right halves of the same embryo. The lines show most recently formed somite boundaries. (B-C) A Mesp1-null embryo (B) shows the same normal somite formation as a wild-type embryo (C). Arrowheads indicate somite boundaries. (D) In Mesp2-null embryos, no somite formation is observed but *Mesp1* is expressed at comparable levels to wild type, although its expression is anteriorly extended and blurred. (E-H) Mesp1-null embryos show normal rostro-caudal patterning of somites. (E,F) Expression of a caudal half marker, *Uncx4.1*. (G,H) Expression of a rostral half marker, *EphA4*. The lines indicate presumptive or formed somite boundaries and the dotted line indicates approximate position of somite half boundary.

3C,D). Mesp2-null cells tended to be eliminated from the epithelial clusters, although they were partially integrated into these structures (blue arrows in Fig. 3C,D). Likewise, small numbers of Mesp2-null cells were found to contribute to the dermomyotome (Fig. 3E,F). Mesp2-null cells also appeared to form the major part of the sclerotome.

Mesp2 is required for the cell-autonomous acquisition of rostral properties

We have previously demonstrated that suppression by Mesp2

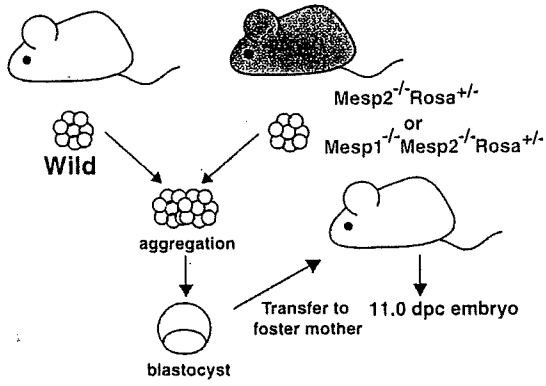

Fig. 2. Schematic representation of chimera analysis method. Either Mesp2-null or Mesp1/Mesp2 double-null embryos, genetically labeled with *Rosa* locus, were aggregated with wild-type embryos at the 8-cell stage, and the resulting chimeras were subjected to analysis at 11.0 dpc.

of the caudal genes *Dll1* and *Uncx4.1* in presumptive rostral half somites is a crucial event in the establishment of the rostro-caudal pattern of somites (Saga et al., 1997; Takahashi et al., 2000). As Mesp2-null embryos exhibit caudalization of somites, Mesp2-null cells are predicted to be unable to express rostral properties. Hence, Mesp2-null cells are expected to distribute to the caudal region of each somite where the rostro-caudal patterns are rescued by wild-type cells in a chimeric embryo. In this context, the localization of Mesp2-null cells at the rostral side was an unexpected finding. We interpret this to mean that the rostral location of Mesp2-null cells is due to a lack of epithelialization functions (see Discussion).

To examine rostro-caudal properties in Mesp2-null cells, located in the rostral side, we analyzed the expression of a caudal half marker gene, *Uncx4.1* (Mansouri et al., 1997; Neidhardt et al., 1997). Analysis of adjacent sections revealed that *lacZ*-expressing Mesp2-null cells, localized at the rostral and central portion, ectopically expressed *Uncx4.1* (Fig. 4A-D). This strongly suggests that Mesp2-null cells cannot acquire rostral properties even if surrounded by wild-type cells, and that Mesp2 function is cell-autonomously required for the acquisition of rostral properties. We also observed that the small number of Mesp2-null cells distributed mostly to the caudal end of the dermomyotome (Fig. 3E,F) and that the expression pattern of *Uncx4.1* was normal in the dermomyotome (Fig. 4E,F). In the sclerotome, *lacZ*-expressing Mesp2-null cells often distributed to the rostral side, where expression of *Uncx4.1* was abnormally elevated (Fig. 4G,H). The vertebrae of the Mesp2-null chimeric fetus showed a partial fusion of the neural arches, which was reminiscent of

Mesp2-hypomorphic fetuses (Fig. 4I,J) (Nomura-Kitabayashi et al., 2002). Fusion of proximal rib elements was also observed (Fig. 4K,L).

Mesp1/Mesp2 double-null cells cannot contribute to the formation of epithelial somites or to the dermomyotome

To address the question of whether Mesp1, in addition to Mesp2, exhibits any function during somitogenesis, we next generated Mesp1/Mesp2 double-null chimeric embryos and compared them with the Mesp2-null chimeric embryos described in the previous sections. We first performed whole-mount X-gal staining of embryos at 11 dpc. In the control chimeric embryo, the X-gal-stained Mesp1/Mesp2 double-heterozygous cells distributed randomly throughout the embryonic body, including the somite region (Fig. 5A,C). By contrast, the Mesp1/Mesp2 double-null chimeric embryo displayed a strikingly uneven pattern of cellular distribution in the somite region. The X-gal stained Mesp1/Mesp2 double-null cells were localized at the medial part of embryonic tail and were not observed in the lateral part of the somite region (Fig. 5B,D). Histological examination of parasagittal sections further revealed obvious differences in the cellular contribution to somite formation (Fig. 5E,F). In the control chimeric embryo, Mesp1/Mesp2 double-heterozygous cells distributed randomly throughout the different stages of somitogenesis (PSM, somite, dermomyotome and sclerotome: Fig. 5E). In the Mesp1/Mesp2 double-null chimeric embryo, neither the initial segment border nor epithelial somites were formed, but histologically distinguishable dermomyotome-like and sclerotome-like compartments were generated (Fig. 5F). In addition, Mesp1/Mesp2 double-null cells and wild-type cells were randomly mixed in the PSM, whereas the dermomyotome-like epithelium consisted exclusively of wild-type cells and the sclerotome-like compartment consisted mostly of Mesp1/Mesp2 double-null cells. This suggests that either Mesp1 or Mesp2 is cell-autonomously required for the formation of epithelial somite and dermomyotome. These results also indicate that PSM cells with different characteristics are rapidly sorted during somite formation.

Subsequent examination of transverse sections confirmed the elimination of Mesp1/Mesp2 double-null cells from dermomyotome (Fig. 5G,H). In the mature somite region, the wild-type dermomyotome-like epithelium was found to form the myotome (my) (Fig. 5I,J). Furthermore, the ventral part of this dermomyotome-like epithelium became mesenchymal and appeared to contribute to the dorsal sclerotome (dsc), implying that this initial dermomyotome-like epithelium actually corresponds to the epithelial somite exclusively composed of wild-type cells (Fig. 5I,J). Fluorescent phalloidin staining revealed that the apical localization of actin filaments is limited to the dorsal compartments, which are occupied by wild-type cells in the Mesp1/Mesp2 double-null chimeric embryo (Fig. 5K,L), indicating the Mesp1/Mesp2 double-null cells cannot undergo epithelialization.

It is known that the bHLH transcription factor paraxis (Tcf15 – Mouse Genome Informatics), is required for the epithelialization of somite and

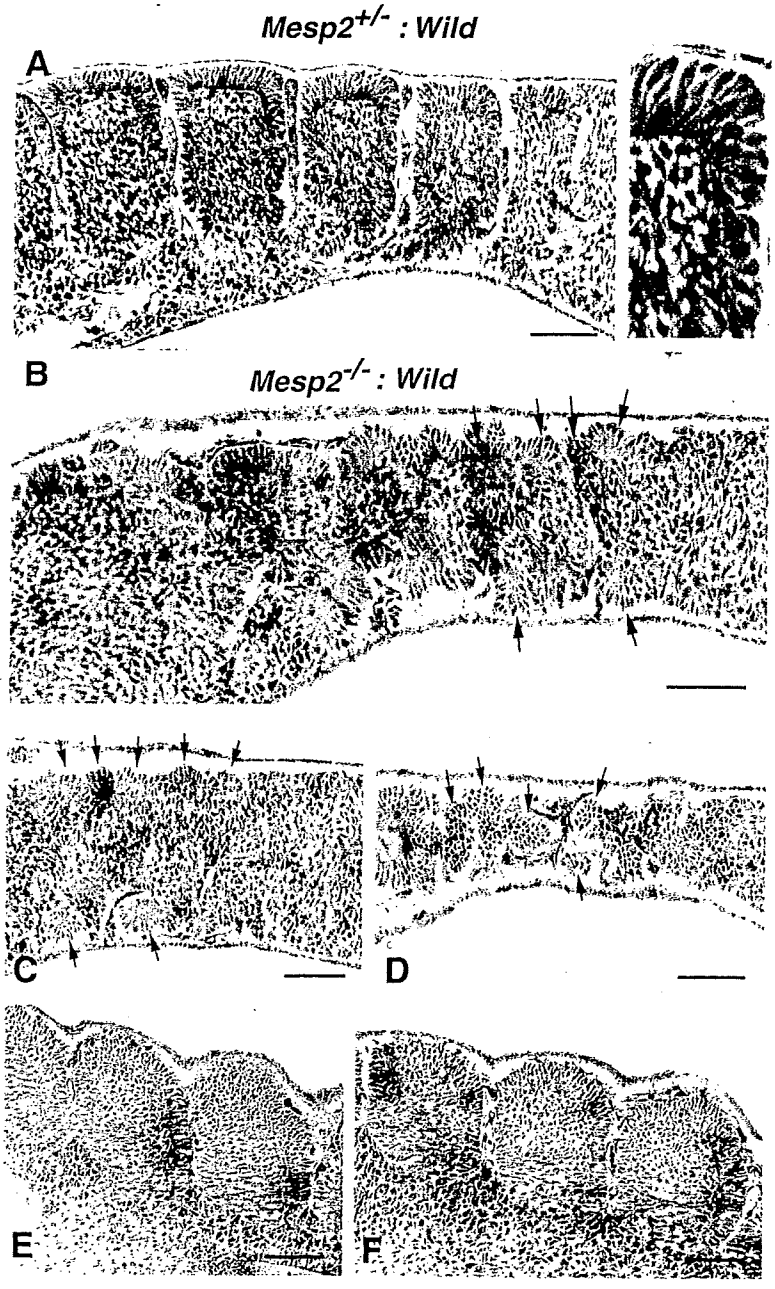

Fig. 3. Mesp2-null cells tend to be excluded from the epithelial region of the somites. (A) The control chimeric embryo undergoes normal somite formation and shows random distribution of labeled cells. The right panel is a high-power view of a somite. (B) In the Mesp2-null chimeric embryo, incompletely segmented somites are formed. Mesp2-null cells tend to be localized at the rostral and central region of these incomplete segments. Red arrows: wild-type cell clusters; blue arrows: Mesp2-null cell clusters. (C,D) Other sections indicating multiple small epithelial cell clusters (arrows). Note that Mesp2-null cells only partially contribute to the epithelial clusters (blue arrows). (E,F) A small number of Mesp2-null cells are distributed in the dermomyotome and are mostly localized at the caudal end. Scale bars: 100 μm.

dermomyotome (Burgess et al., 1995; Burgess et al., 1996). Although *Paraxis* expression is not affected in Mesp2-null embryos (data not shown), it is possible that it is influenced by the loss of both Mesp1 and Mesp2. We therefore examined the expression patterns of *Paraxis* in our Mesp1/Mesp2 double-null chimeras. In wild-type embryos *Paraxis* is initially expressed throughout the entire somite region (in both the prospective dermomyotomal and sclerotomal regions) in the anteriormost PSM and newly forming somites, and then localizes in the dermomyotomes (Burgess et al., 1995). The dorsal dermomyotomal epithelium, composed of wild-type cells, strongly expressed *Paraxis* in the chimeric embryo (Fig. 6A,B). In addition, adjacent sections revealed that *lacZ*-expressing Mesp1/Mesp2 double-null cells expressed *Paraxis* in the medial sclerotomal compartment (Fig. 6A,B, brackets). This suggests that *Paraxis* expression in the future sclerotomal region is independent of Mesp factors. However, at present we cannot exclude the possibility that the maintenance of *Paraxis* expression in the dermomyotome requires the functions of either Mesp1 or Mesp2.

Mesp1/Mesp2 double-null cells are incapable of acquiring rostral properties

To clarify the rostro-caudal properties of somites in our chimeric embryos, we examined the expression pattern of *Uncx4.1*. Control chimeric embryos exhibited a normal stripe pattern of *Uncx4.1* expression throughout the segmented somite region (Fig. 7A). By contrast, Mesp1/Mesp2 double-null chimeric embryos exhibited continuous *Uncx4.1* expression in the ventral sclerotomal region (Fig. 7B). This continuity was observed in the entire sclerotome-like compartment of the newly formed somite region and in the ventral sclerotome in the mature somite region. The caudal localization of *Uncx4.1* expression, however, was normal in the dermomyotome and the dorsal sclerotome, which consisted of wild-type cells (Fig. 5), even in Mesp1/Mesp2 double-null chimeras. This suggests that, like Mesp2-null cells, Mesp1/Mesp2 double-null cells are incapable of acquiring rostral properties. Since the mesoderm of Mesp1/Mesp2 double-null embryos lacks the expression of the major markers of paraxial mesoderm (Kitajima et al., 2000), and Mesp1/Mesp2 double-null cells do not exhibit histological features characteristic of epithelial somites in our current study, it is possible that Mesp1/Mesp2 double-null cells may lack paraxial mesoderm properties. However, the analysis of adjacent sections suggests that *lacZ*-expressing Mesp1/Mesp2 double-null cells themselves express *Uncx4.1*, a somite-specific marker (Fig. 7C,D), and they had also been found to have normal expression of *Paraxis* (Fig. 6A,B).

It is believed that the rostro-caudal pattern within somites and dermomyotomes is generated in the PSM and maintained in somites and dermomyotomes. We observed a normal rostro-caudal pattern in the dermomyotome (Fig. 7), although wild-type cells and Mesp1/Mesp2 double-null cells are mixed in the PSM (Fig. 5), of Mesp1/Mesp2 double-null chimeric embryos. As Mesp products are required for suppression of *Dll1* in the anterior PSM, a normal Dll1 stripe pattern cannot be formed if Mesp1/Mesp2 double-null cells are randomly distributed in

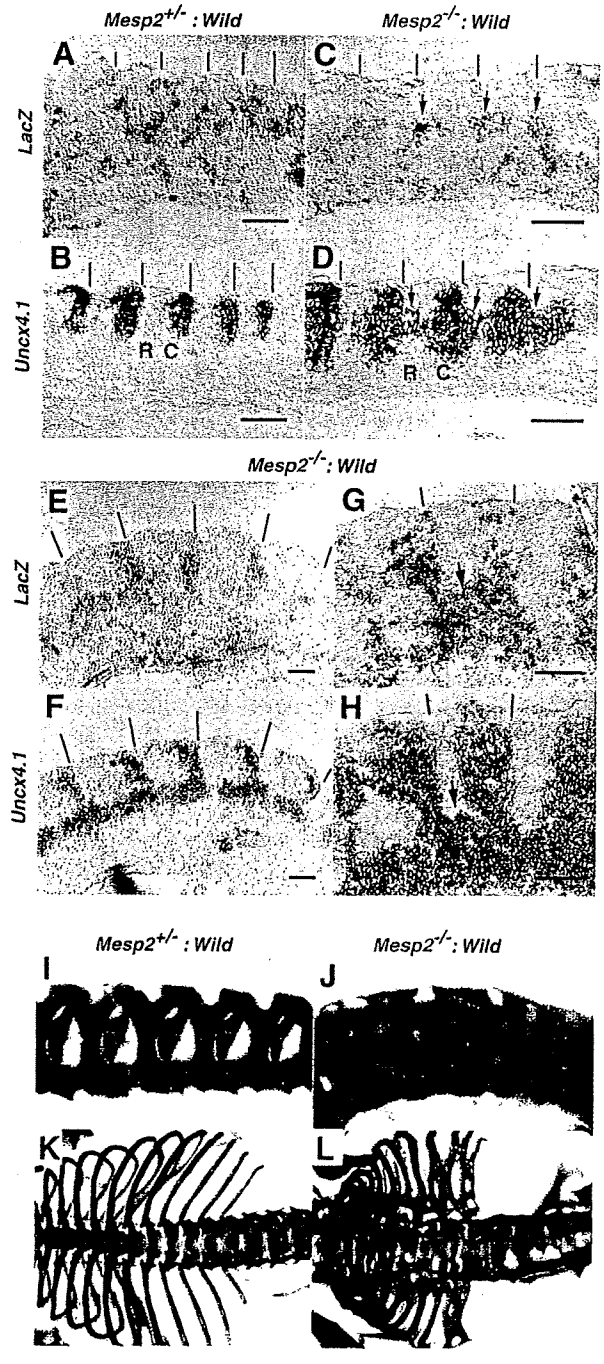

Fig. 4. Mesp2 function is cell autonomously required for rostral properties. (A-D) Expression of *lacZ* and *Uncx4.1* transcripts at the site of initial somite formation in control (A,B) and Mesp2-null (C,D) chimeric embryos. In the control, *lacZ*-expressing cells are randomly distributed and *Uncx4.1* expression is normal. In the Mesp2-null chimera, *lacZ*-expressing Mesp2-null cells at the rostral part of the incomplete segments (arrows in C) ectopically express *Uncx4.1* (arrows in D). Lines indicate somite boundaries. (E,F) In the dermomyotome, Mesp2-null cells are mostly localized at the caudal end, and the *Uncx4.1* expression pattern is normal. (G,H) In the sclerotome, the distribution of Mesp2-null cells results in expansion of *Uncx4.1* expression (arrows). (I) The control chimeric fetus shows normal vertebrae. (J) The Mesp2-null chimeric fetus exhibits partial fusion of the neural arches. (K) The control chimeric fetus shows normal ribs. (L) The Mesp2-null chimeric fetus shows proximal rib fusion. Scale bars: 100 μm. C, caudal compartment; R, rostral compartment.

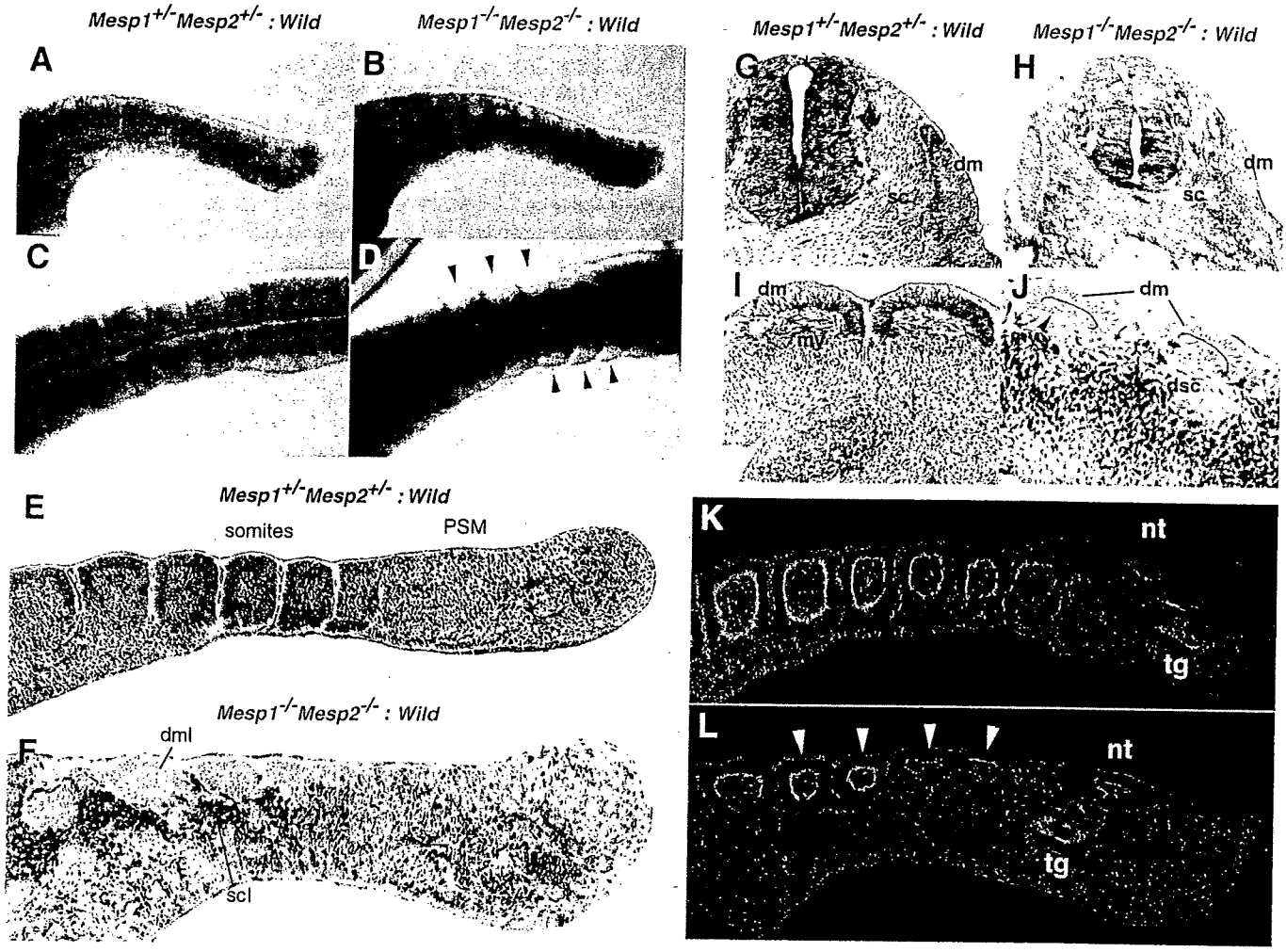

Fig. 5. Mesp1/Mesp2 double-null cells fail to contribute to epithelial somites or to the dermomyotome. (A-D) Tail regions from X-gal-stained whole-mount specimens of control (A,C) and double-null (B,D) chimeric embryos. (A,B) Lateral view. (C,D) Dorsal view. The blue double-heterozygous cells are randomly distributed in the control embryo, whereas the Mesp1/Mesp2 double-null cells are excluded from the lateral region of the somites (arrowheads in D). (E,F) Parasagittal sections of tails from chimeric embryos. (E) The labeled cells are randomly located in the control chimera. (F) The two types of cells are randomly mixed in the PSM, whereas the dermomyotome-like epithelium consisted exclusively of wild-type cells and the sclerotome-like compartment contained mostly Mesp1/Mesp2 double-null cells. Note that normal epithelial somites are not formed in this chimera. (G,H) Transverse sections show elimination of Mesp1/Mesp2 double-null cells from the dermomyotome. (I,J) The dermomyotome-like epithelium in the Mesp1/Mesp2 double-null chimeric embryo gives rise to dermomyotome, myotome (arrowhead in J) and the dorsal part of the sclerotome. Red arches indicate the inner surface of dermomyotome. (K,L) AlexaFluor 488-labeled phalloidin staining shows normal epithelialization of somites in the control chimera (K) and restriction of epithelialization in the dermomyotome-like compartment in the Mesp1/Mesp2 double-null chimera (L). dm, dermomyotome; dml, dermomyotome-like epithelium; dsc, dorsal part of the sclerotome; my, myotome; nt, neural tube; sc, sclerotome; scl, sclerotome-like compartment; tg, tail gut.

the anterior PSM. This is because 50% of cells cannot undergo suppression of Dll1 even in the future rostral half region. Therefore, our finding of a normal rostro-caudal pattern in the dermomyotome of double-null chimeras is surprising and raises the question of whether wild-type cells can be normally patterned in the presence of surrounding Mesp1/Mesp2 double-null cells. To determine how the rostro-caudal pattern in the dermomyotome is formed in the PSM, we examined the expression pattern of *Dll1* (Bettenhausen et al., 1995), the stripe expression profile of which is established in the anteriormost PSM via the function of Mesp2 (Takahashi et al., 2000). The *lacZ*-expressing Mesp1/Mesp2 double-null cells were subsequently found to be consistently localized in the sclerotome-like region, where *Dll1* expression was abnormally expanded (Fig. 6C,D). In the dermomyotome-like region, however, *Dll1* expression in the caudal half was normal. Intriguingly, strong *Dll1* expression in the anteriormost PSM was suppressed in a rostrally adjoining cell population, which is mainly occupied by wild-type cells (Fig. 6C,D, arrows). This implies that wild-type cells and Mesp1/Mesp2 double-null cells rapidly segregate at S–1 to S0, after which the rostro-caudal pattern of *Dll1* expression is formed in the partially segregated wild-type cell population but not in the randomly mixed cell population. In other words, the separation from Mesp1/Mesp2 double-null cells enabled normal rostro-caudal patterning of wild-type cells.

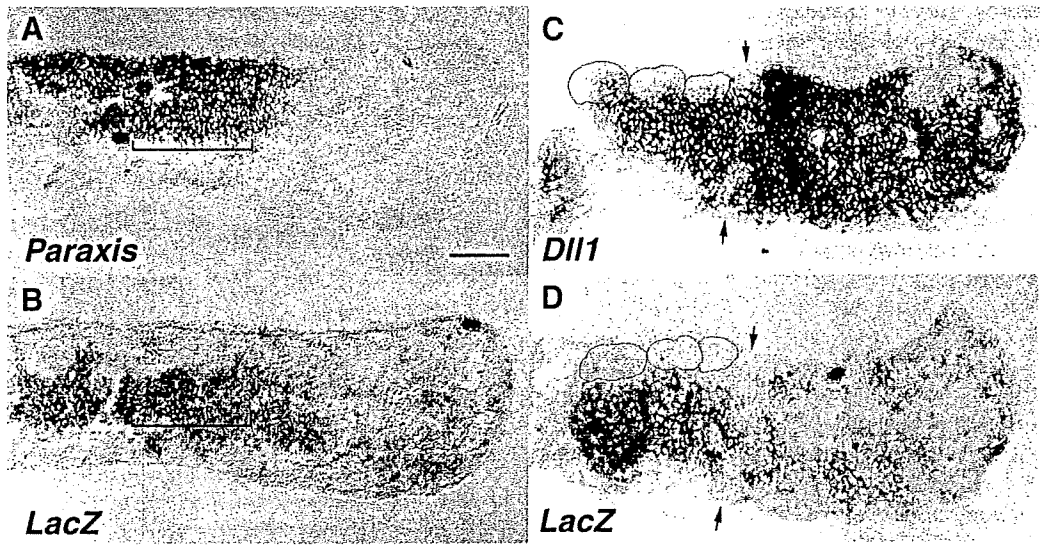

Fig. 6. (A,B) Mesp1/Mesp2 double-null cells express *Paraxis*. Adjacent parasagittal sections of the Mesp1/Mesp2 double-null chimeric embryo were stained for either *Paraxis* (A) or *lacZ* (B). Note that the expression domains of the two genes overlap in the medial sclerotomal region (brackets). (C,D) The rostro-caudal pattern in the dermomyotome is formed in a partially segregating wild-type cell population. Adjacent sections of the Mesp1/Mesp2 double-null chimeric embryos were stained for *Dll1* (C) or *lacZ* (D) mRNA. Red outlines demarcate the dorsal dermomyotome-like compartments. Note that suppression of *Dll1* expression occurs in a region mostly occupied by wild-type cells (arrows). Scale bar: 100 μm.

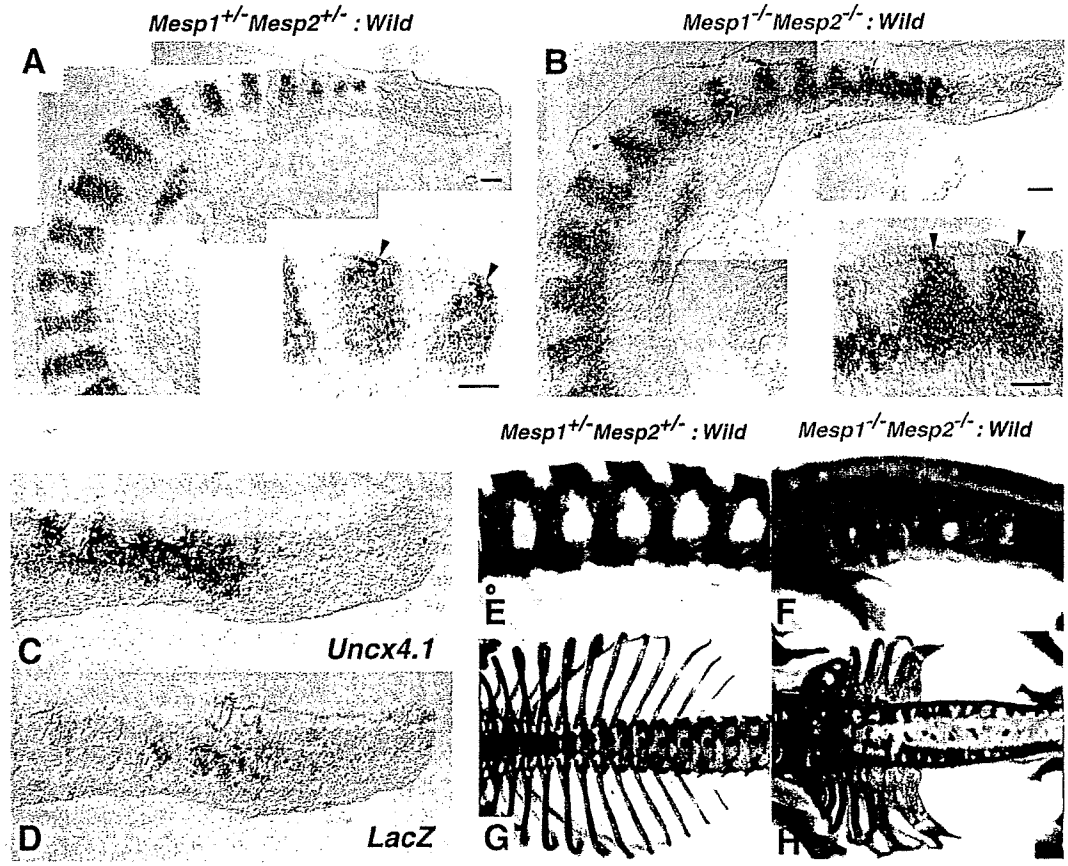

Fig. 7. Rostro-caudal patterning of the sclerotome is disrupted in Mesp1/Mesp2 double-null chimeric embryos. (A) The control chimeric embryos exhibit normal stripe patterns of *Uncx4.1* expression throughout the somite region. (B) The Mesp1/Mesp2 double-null chimeric embryos exhibit continuous *Uncx4.1* expression in the ventral sclerotomal region. Note that caudal localization of *Uncx4.1* expression is normal in the dermomyotome and dorsal sclerotome. The insets show a higher magnification of lumbar somites. (C,D) Adjacent sections showing that *lacZ*-expressing Mesp1/Mesp2 double-null cells express *Uncx4.1*. (E-H) The Mesp1/Mesp2 double-null chimeric fetus exhibits caudalization of the vertebrae and of the proximal ribs. (E) The control chimeric fetus shows normal metameric arrangement of the neural arches. (F) The Mesp1/Mesp2 double-null chimeric fetus shows severe fusion of the pedicles and the laminae of neural arches. (G) The control chimeric fetus has normal arrangement of ribs. (H) The double-null chimeric fetus shows severe fusion of the proximal elements of the ribs. Scale bars: 100 μm.

Mesp2-null fetuses display caudalized vertebrae with extensive fusion of the pedicles of neural arches and proximal elements of the ribs (Saga et al., 1997). The Mesp1/Mesp2 double-null chimeric fetuses also exhibited fusion of the pedicles of neural arches and the proximal ribs (Fig. 7E-H). Furthermore, the vertebrae of severe chimeric fetuses were indistinguishable from those of Mesp2-null fetuses. These observations indicate that Mesp1/Mesp2 double-null cells can differentiate into caudal sclerotome and possibly contribute to chondrogenesis.

Discussion

Mesp1 and Mesp2 not only exhibit similar expression patterns but also share common bHLH domains as transcription factors. Previous studies using gene replacement experiments (Saga, 1998) (Y.S. and S.K., unpublished) indicate that these genes can compensate for each other. However, the early lethality of double knockout mice hampered any further detailed analysis of somitogenesis. An obvious strategy to further elucidate the functions of Mesp1 and Mesp2 was, therefore, the generation of a conditional knockout allele for *Mesp2* in *Mesp1* disrupted cells in which the Cre gene is specifically activated in the paraxial mesoderm, which is now underway. Chimera analysis is also a powerful method as an alternative strategy. Comparisons of chimeras, composed of either Mesp2-null or Mesp1/Mesp2 double-null cells, made it possible to determine the contribution of Mesp1 to somitogenesis. Our results indicate that Mesp1 has redundant functions in the epithelialization of somitic mesoderm and additionally, by chimeric analysis, we were able to demonstrate the cell autonomy of Mesp1 and Mesp2 function during some critical steps of somitogenesis.

The relative contributions of Mesp1 and Mesp2 to somitogenesis

In Mesp1-null mice, epithelial somites with normal rostro-caudal polarity are generated, whereas Mesp2-null mice exhibit defects in both the generation of epithelial somites and the establishment of rostro-caudal polarity. Thus, it seems likely that Mesp2 function is both necessary and sufficient for somitogenesis. However, dermomyotome formation was observed, without normal segmentation, even in Mesp2-null mice. In view of the apparent redundant functions of Mesp1 and Mesp2 in somitogenesis, as demonstrated by our previous gene replacement study, it was possible that the Mesp1/Mesp2 double-null embryo would exhibit a much more severe phenotype in relation to somitogenesis. In our chimera analyses, both Mesp2-null and Mesp1/Mesp2 double-null cells exhibited complete caudalization of somitic mesoderm, indicating that Mesp1 function is not sufficient to rescue Mesp2 deficiency and restore rostro-caudal polarity. Likewise, both Mesp2-null and Mesp1/Mesp2 double-null cells were incapable of forming an initial segment boundary, showing that the contribution of Mesp1 is also minor during this process. By contrast, whereas Mesp1/Mesp2 double-null cells lacked any ability to epithelialize, Mesp2-null cells were occasionally integrated into epithelial somites and dermomyotome, indicating that the contribution of Mesp1 to epithelialization is significant and that Mesp1 can function in the absence of Mesp2 (Fig. 8). We therefore postulate that the epithelialization of dermomyotome, observed in Mesp2-null embryos, is dependent on Mesp1.

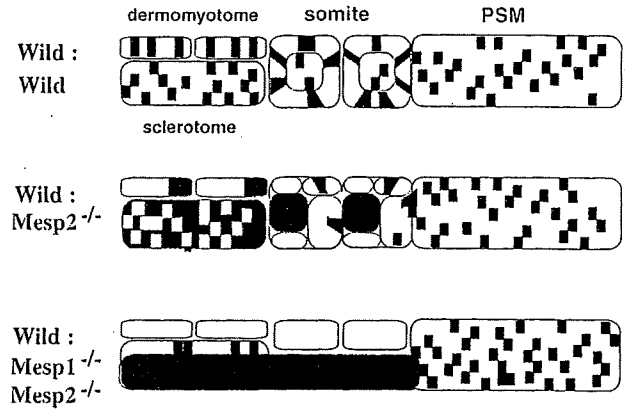

Fig. 8. A schematic summarization of the Mesp1/Mesp2 chimera experiments. Mesp1/Mesp2 double-null cells can contribute to neither epithelial somite nor dermomyotome formation, whereas Mesp2-null cells can partially contribute to both somites and dermomyotome. Red outlines indicate epithelialized tissues (epithelial somites, dermomyotomes and abnormal small clusters).

Mesp factors are cell autonomously required for epithelialization of somitic mesoderm but may also be non-cell autonomously required for morphological boundary formation

Conventional interpretations of the results of chimera analysis are generally based upon the regulative development of the vertebrate embryo and argue cell autonomy of specific gene functions in embryogenesis (Ciruna et al., 1997; Brown et al., 1999; Kitajima et al., 2000; Koizumi et al., 2001). Mesp1/Mesp2 double-null cells failed to form epithelial somites, even in the presence of surrounding wild-type cells. In addition, they were incapable of contributing to dermomyotome, where cell sorting occurs. This strongly suggests that Mesp factors are cell autonomously required for the epithelialization of somitic mesoderm. However, we also found striking non-cell autonomous effects of Mesp mutant cells on wild-type cell behaviors. That is, both types of Mesp mutant cell not only failed to undergo normal somitogenesis, but also inhibited the normal morphogenesis of wild-type cells. This implies that there are non-cell autonomous roles for Mesp factors in the establishment of the future somite boundary, as we will discuss further.

Initial epithelial somite formation is achieved by the mesenchymal-epithelial transition of cells located in the anterior PSM. A future somite boundary is established at a specific position in the PSM, followed by gap formation between the mesenchymal cell populations. Subsequently, cells located anterior to the boundary are epithelialized. This process is known to be mediated by an inductive signal from cells posterior to the boundary (Sato et al., 2002). Therefore, defects in epithelial somite formation can be explained in two principal ways: a lack of cellular ability to epithelialize (cell autonomous) and a lack of an inducing signal, which is produced in the anterior PSM by a mechanism mediated by Notch signaling (thus non-cell autonomous). In the case of chimeras of Mesp1/Mesp2 double-null cells, no local

boundary formed by locally distributed wild-type cells was observed, i.e. even a gap between wild-type cells was never observed in the mixture of Mesp1/Mesp2 double-null cells and wild-type cells. It is likely, therefore, that the wild-type cell population can form a boundary only after separation from Mesp1/Mesp2 double-null cells (Fig. 8). By contrast, some local boundaries between epithelial wild-type cell clusters were occasionally observed in chimeras with Mesp2-null cells. Considering that there is functional redundancy between these transcription factors, it is possible that either Mesp1 or Mesp2 is necessary for the formation of a signaling center or source of the putative inductive signal. Hence, we cannot exclude the possibility that the lack of Mesp function may affect non-cell autonomous generation of the inductive signal in the anterior PSM.

Formation of epithelial somites requires paraxis, which is a transcription factor (Burgess et al., 1996; Nakaya et al., 2004). We observed that Mesp1/Mesp2 double-null cells at the medial sclerotomal region expressed *Paraxis*, indicating that Mesp factors are not absolutely required for *Paraxis* expression. Defects in epithelial somite formation in paraxis-null embryos, with normal *Mesp2* expression (Johnson et al., 2001), and in Mesp2-null embryos, with normal *Paraxis* expression, imply that epithelial somite formation independently requires both gene functions.

Mesp2 is cell autonomously required for the acquisition of rostral properties

The distribution of Mesp2-null cells in the Mesp2-null chimeric embryos may appear somewhat paradoxical, as they are localized at the rostral side in the incomplete somites but at the caudal side in the dermomyotome. Initial localization at the rostral and central region, however, is likely to be due to the relative lack of epithelialization functions. In mammalian and avian embryos, mesenchymal-to-epithelial conversion of the PSM commences from the rostral side of the future somite boundary, i.e. the caudal margin of the presumptive somite (Duband et al., 1987). Epithelialization then proceeds anteriorly in the dorsal and ventral faces and in such a process, Mesp2-null cells, which are less able to participate in epithelialization, may therefore be pushed to the central and rostral sides. Thus, the majority of the Mesp2-null cells localize to the central, prospective sclerotomal region and a small number of them are integrated in the future dermomyotomal region. The incomplete somites then undergo reorganization into dermomyotome and sclerotome, and small numbers of Mesp2-null cells in the dermomyotome may be sorted out to the caudal end. Therefore, the apparently complex distribution pattern of Mesp2-null cells is likely to reflect a combination of defects in epithelialization and rostro-caudal patterning. In the incomplete segments of Mesp2-null chimeric embryos, the Mesp2-null cells fail to acquire rostral properties even when localized at the rostral side. Moreover, in the dermomyotome, where rostro-caudal patterning is rescued, Mesp2-null cells are mostly localized in the caudal region. These observations suggested that the requirement of Mesp2 for the acquisition of rostral properties is cell autonomous. Similarly, it has been reported that presenilin 1 (Psen1) is required for acquisition of caudal half properties (Takahashi et al., 2000; Koizumi et al., 2001) and that Psen1-null cells cannot contribute to the caudal half of somites in chimeric embryos, showing cell autonomous roles for Psen1 (Koizumi et al., 2001).

Mesp mutant cells affect the rostro-caudal patterning of somites due to the lack of cellular interaction with wild-type cells

In a previous study, we have shown that the rostro-caudal patterning of somites is generated by complex cellular interactions involved in positive and negative feedback pathways of Dll1-Notch and Dll3-Notch signaling, and regulation by Mesp2 in the PSM (Takahashi et al., 2003). In chimeras with either Mesp2-null or Mesp1/Mesp2 double-null cells, the mutant cells were distributed evenly and did not show any sorting bias in a rostro-caudal direction in the PSM. Since both Mesp2-null and Mesp1/Mesp2 double-null cells have the ability to form caudal cells, it is likely that if wild-type cells could occupy the rostral part of future somite regions and have the ability to sort in the PSM, a normal rostro-caudal patterning would be generated. We did not observe this, however, and conclude that the presence of mutant cells lacking Mesp factors must have disrupted normal cellular interactions via Notch signaling. Thus these non-cell-autonomous effects of our mutant cells are strongly supportive of our previous contention that rostro-caudal pattering is generated by cellular interactions via Notch signaling.

We thank Mariko Ikumi, Seiko Shinzawa, Eriko Ikeno and Shinobu Watanabe for general technical assistance. This work was supported by Grants-in-Aid for Science Research on Priority Areas (B) and the Organized Research Combination System of the Ministry of Education, Culture, Sports, Science and Technology, Japan.

References

Bettenhausen, B., Hrabe de Angelis, M., Simon, D., Guénet, J.-L. and Gossler, A. (1995). Transient and restricted expression during mouse embryogenesis of Dll1, a murine gene closely related to *Drosophila* Delta. *Development* **121**, 2407-2418.

Borycki, A. G. and Emerson, C. P., Jr (2000). Multiple tissue interactions and signal transduction pathways control somite myogenesis. *Curr. Top. Dev. Biol.* **48**, 165-224.

Brown, D., Wagner, D., Li, X., Richardson, D. A. and Olson, E. N. (1999). Dual role of the basic helix-loop-helix transcription factor scleraxis in mesoderm formation and chondrogenesis during mouse embryogenesis. *Development* **126**, 4317-4329.

Burgess, R., Cserjesi, P., Ligon, K. L. and Olson, E. N. (1995). Paraxis: a basic helix-loop-helix protein expressed in paraxial mesoderm and developing somites. *Dev. Biol.* **168**, 296-306.

Burgess, R., Rawls, A., Brown, D., Bradley, A. and Olson, E. N. (1996). Requirement of the *paraxis* gene for somite formation and musculoskeletal patterning. *Nature* **384**, 570-573.

Ciruna, B. G., Schwartz, L., Harpal, K., Yamaguchi, T. P. and Rossant, J. (1997). Chimeric analysis of *fibroblast growth factor receptor-1 (Fgfr1)* function: a role for FGFR1 in morphogenetic movement through the primitive streak. *Development* **124**, 2829-2841.

Duband, J. L., Dufour, S., Hatta, K., Takeichi, M., Edelman, G. M. and Thiery, J. P. (1987). Adhesion molecules during somitogenesis in the avian embryo. *J. Cell Biol.* **104**, 1361-1374.

Fan, C. M. and Tessier Lavigne, M. (1994). Patterning of mammalian somites by surface ectoderm and notochord: Evidence for sclerotome induction by a hedgehog homolog. *Cell* **79**, 1175-1186.

Gossler, A. and Hrabe de Angelis, M. (1997). Somitogenesis. *Curr. Top. Dev. Biol.* **38**, 225-287.

Johnson, J., Rhee, J., Parsons, S. M., Brown, D., Olson, E. N. and Rawls, A. (2001). The anterior/posterior polarity of somites is disrupted in Paraxis-deficient mice. *Dev. Biol.* **229**, 176-187.

Kitajima, S., Takagi, A., Inoue, T. and Saga, Y. (2000). MesP1 and MesP2

are essential for the development of cardiac mesoderm. *Development* **127**, 3215-3226.

Koizumi, K., Nakajima, M., Yuasa, S., Saga, Y., Sakai, T., Kuriyama, T., Shirasawa, T. and Koseki, H. (2001). The role of presenilin 1 during somite segmentation. *Development* **128**, 1391-1402.

Mansouri, A., Yokota, Y., Wehr, R., Copeland, N. G., Jenkins, N. A. and Gruss, P. (1997). Paired-related murine homeobox gene expressed in the developing sclerotome, kidney, and nervous system. *Dev. Dyn.* **210**, 53-65.

Nakaya, Y., Kuroda, S., Katagiri, Y. T., Kaibuchi, K. and Takahashi, Y. (2004). Mesenchymal-epithelial transition during somitic segmentation is regulated by differential roles of Cdc42 and Rac1. *Dev. Cell* **7**, 425-438.

Neidhardt, L. M., Kispert, A. and Herrmann, B. G. (1997). A mouse gene of the paired-related homeobox class expressed in the caudal somite compartment and in the developing vertebral column, kidney and nervous system. *Dev. Genes Evol.* **207**, 330-339.

Nieto, M. A., Gilardi-Hebenstreit, P., Charnay, P. and Wilkinson, D. G. (1992). A receptor protein tyrosine kinase implicated in the segmental patterning of the hindbrain and mesoderm. *Development* **116**, 1137-1150.

Nomura-Kitabayashi, A., Takahashi, Y., Kitajima, S., Inoue, T., Takeda, H. and Saga, Y. (2002). Hypomorphic *Mesp* allele distinguishes establishment of rostro-caudal polarity and segment border formation in somitogenesis. *Development* **129**, 2473-2481.

Pourquié, O. (2001). Vertebrate somitogenesis. *Annu. Rev. Cell. Dev. Biol.* **17**, 311-350.

Saga, Y. (1998). Genetic rescue of segmentation defect in MesP2-deficient mice by MesP1 gene replacement. *Mech. Dev.* **75**, 53-66.

Saga, Y. and Takeda, H. (2001). The making of the somite: molecular events in vertebrate segmentation. *Nat. Rev. Genet.* **2**, 835-845.

Saga, Y., Hata, N., Kobayashi, S., Magnuson, T., Seldin, M. and Taketo, M. M. (1996). MesP1: A novel basic helix-loop-helix protein expressed in the nascent mesodermal cells during mouse gastrulation. *Development* **122**, 2769-2778.

Saga, Y., Hata, N., Koseki, H. and Taketo, M. M. (1997). *Mesp2*: a novel mouse gene expressed in the presegmented mesoderm and essential for segmentation initiation. *Genes Dev.* **11**, 1827-1839.

Saga, Y., Miyagawa-Tomita, S., Takagi, A., Kitajima S., Miyazaki, J. and Inoue, T (1999). MesP1 is expressed in the heart precursor cells and required for the formation of a single heart tube. *Development* **126**, 3437-3447.

Sato, Y., Yasuda, K. and Takahashi, Y. (2002). Morphological boundary forms by a novel inductive event mediated by Lunatic fringe and Notch during somitic segmentation. *Development* **129**, 3633-3644.

Takahashi, Y., Koizumi, K., Takagi, A., Kitajima, S., Inoue, T., Koseki, H. and Saga, Y. (2000). Mesp2 initiates somite segmentation through the Notch signalling pathway. *Nat. Genet.* **25**, 390-396.

Takahashi, Y., Inoue, T., Gossler, A. and Saga, Y. (2003). Feedback loops comprising Dll1, Dll3 and Mesp2, and differential involvement of Psen1 are essential for rostrocaudal patterning of somites. *Development* **130**, 4259-4268.

Zambrowicz, B. P., Imamoto, A., Fiering, S., Herzenberg, L. A., Kerr, W. G. and Soriano, P. (1997). Disruption of overlapping transcripts in the ROSA beta geo 26 gene trap strain leads to widespread expression of beta-galactosidase in mouse embryos and hematopoietic cells. *Proc. Natl. Acad. Sci. USA* **94**, 3789-3794.

ELSEVIER

Mechanisms of Development 121 (2004) 1443–1453

www.elsevier.com/locate/modo

Mouse Nkd1, a Wnt antagonist, exhibits oscillatory gene expression in the PSM under the control of Notch signaling

Aki Ishikawa[a], Satoshi Kitajima[b], Yu Takahashi[b], Hiroki Kokubo[a], Jun Kanno[b], Tohru Inoue[b], Yumiko Saga[a,*]

[a]*Division of Mammalian Development, National Institute of Genetics, Yata 1111, Mishima 411-8540, Japan*
[b]*Cellular and Molecular Toxicology Division, National Institute of Health Sciences, 1-18-1 Kamiyoga, Setagayaku, Tokyo 158-8501, Japan*

Received 19 May 2004; received in revised form 29 July 2004; accepted 9 August 2004
Available online 16 September 2004

Abstract

During vertebrate embryogenesis, the formation of reiterated structures along the body axis is dependent upon the generation of the somite by segmentation of the presomitic mesoderm (PSM). Notch signaling plays a crucial role in both the generation and regulation of the molecular clock that provides the spatial information for PSM cells to form somites. In a screen for novel genes involved in somitogenesis, we identified a gene encoding a Wnt antagonist, Nkd1, which is transcribed in an oscillatory manner, and may represent a new member of the molecular clock constituents. The transcription of *nkd1* is extremely downregulated in the PSM of *vestigial tail* (*vt/vt*), a hypomorphic mutant of Wnt3a, whereas *nkd1* oscillations have a similar phase to *lunatic fringe* (*L-fng*) transcription and they are arrested in Hes7 (a negative regulator of Notch signaling) deficient embryos. These results suggest that the transcription of *nkd1* requires Wnt3a, and that its oscillation patterns depend upon the function of Hes7. Wnt signaling has been postulated to be upstream of Notch signaling but we demonstrate in this study that a Wnt-signal-related gene may also be regulated by Notch signaling. Collectively, our data suggest that the reciprocal interaction of Notch and Wnt signals, and of their respective negative feedback loops, function to organize the segmentation clock required for somitogenesis.

Keywords: Subtraction; Somitogenesis; Wnt signaling; Mesp2; Segmentation clock

1. Introduction

Somites are transient structures that are only observed during embryogenesis, and their reiterated nature in vertebrates is an important foundation for the generation of metameric structures such as vertebrae, ribs, spinal nerves and skeletal muscle. The somites are formed sequentially in an anterior to posterior direction, concomitant with the posterior extension of the tailbud. Once the paraxial mesoderm is generated from the tailbud, the cells are known to then be under the control of the segmentation clock (or molecular clock) and acquire periodic properties (Pourquié, 2001). Among the several genes that have been implicated in somitogenesis, those involved in the Notch signaling pathway are now known to play major roles. The experimental and genetic evidence that is now accumulating also indicates that Notch signaling is a component of the molecular clock that governs temporal control, and that it is also required for the establishment of the rostro-caudal polarity of somites within the presomitic mesoderm (PSM) prior to segment border formation (Takahashi et al., 2000). The molecular mechanisms underlying these events have recently begun to be more fully understood. There could, however, be additional genes and/or signaling pathways involved in somitogenesis. In fact, Wnt signaling is implicated in both the generation and maturation of tailbud cells (Takada et al., 1994), whereas FGF signaling has been shown to be important for the maintenance of immature PSM cells prior to segmentation (Dubrulle et al., 2001; Sawada, 2001).

Previously, we cloned the gene *Mesp2*, which encodes a bHLH-type transcription factor (Saga et al., 1997) and is

* Corresponding author. Tel: +81-559-81-6829; fax: +81-559-81-6828.
E-mail address: ysaga@lab.nig.ac.jp (Y. Saga).

0925-4773/$ - see front matter © 2004 Elsevier Ireland Ltd. All rights reserved.
doi:10.1016/j.mod.2004.08.003

transiently expressed in the rostral PSM (in either S-1 or S-2: we refer a forming somite as S0) before segment border formation occurs. Additionally, *Mesp2*-null mice show defective somitogenesis due to a lack of a rostral somitic compartment. Recent genetic analyses have also now revealed that *Mesp2* functions in a Notch-signaling feedback network (Takahashi et al., 2003). Mesp2 stimulates *Notch1* expression and suppresses *Dll1* expression, whereas both Notch 1 and Dll1 appear to be required for either the activation or maintenance of *Mesp2* expression. However, no direct targets of Mesp2 have yet been identified.

In order to identify putative downstream target genes of Mesp2 and to further elucidate the molecular mechanisms underlying the formation and maturation of PSM cells, which are required for somite segmentation, we generated two subtractive cDNA libraries and screened them by in situ hybridization (ISH). We subsequently obtained more than 30 clones that are expressed in either the somite, the PSM and/or the tailbud. Among these genes, we identified several known components of the Wnt signaling pathway, and we focused in particular on the mouse *nkd1* gene which is expressed in an oscillatory manner in the PSM. *nkd* is a homolog of the *Drosophila* segment polarity gene *naked cuticle* (*nkd*), which encodes an antagonist of Wg activity (Zeng et al., 2000). It has been shown that mouse Nkd1 can bind Dishevelled and antagonize canonical Wnt signaling (Yan et al., 2001a; Wharton et al., 2001). Furthermore, it has also recently been reported that *Axin2*, which encodes an inhibitor of Wnt signaling, exhibits a cyclic expression pattern during somitogenesis and may play a key role upstream of the segmentation clock generated by Notch signaling (Aulehla et al., 2003). Our comparative analyses of such cyclic genes suggest that *nkd1* is a component of these pathways that exhibits an oscillatory expression pattern, which may act as a link between the Notch and Wnt signaling cascades and contribute to the establishment of the segmentation clock.

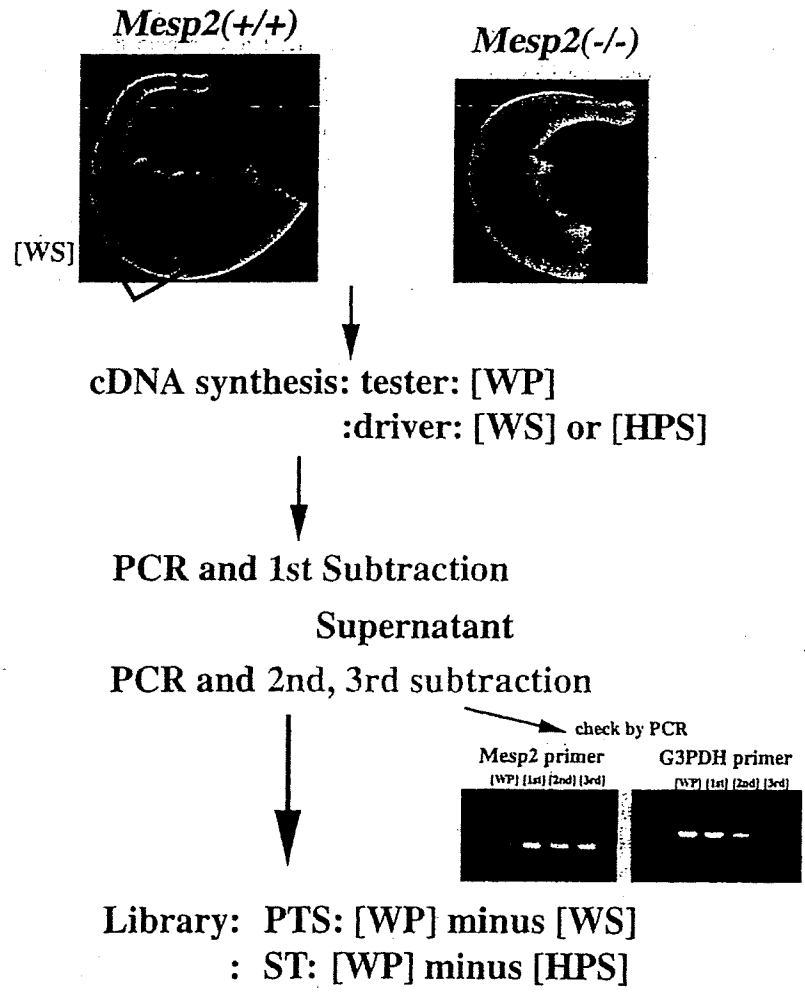

Fig. 1. Schematic representation of subtractive cDNA library protocols. Subtraction was carried out with cDNAs derived from the dissected portions of either wild-type (WP and WS) or Mesp2-null (HPS) 11.5 dpc embryos. Two different types of oligonucleotide linker-primers were utilized to prepare either tester or driver cDNAs. After three rounds of subtraction, the efficiency of the method was validated for the *Mesp2* (specific RNA to the PSM) and *G3PDH* (ubiquitous

Table 1
Characterization of somitic genes obtained using the subtractive strategy

Clone no.	Character	EP in WT	EP in Mesp2$^{-/-}$
ST347	Hes7	PSM (oscillates)	No change
ST371	laminin alpha 1	PSM (strong at S-1)	Expands anteriorly
ST556	Glcci1*	AER, somite, NT (dorsal)	No change
ST623	Laminin 5	PSM-1, somite anterior	Disappears
ST676	LEF1	PSM	Expands ante-
ST686		(strong at S-1)	riorly (S-1 region)
ST762			
PTS286			
PTS360			
ST313	Neuropilin-2	Rostral compartment of somites	Disappears
ST736	Axin2	PSM (oscillates) (S-1 region)	Expands anteriorly (S-1 region)
PTS124	SemaF-Cap3	PSM, somite	Downregulated
PTS338			
PTS149	DOC4/Nrg1	PSM, somite, head	No change
PTS179	Slit3	Tailbud, somite, DM	No change
PTS250	Hoxc13	Tailbud	No change
PTS426			
PTS607			
PTS363	Tropomyosin	Tailbud	No change
PTS378#	No gene prediction	PSM(S-1)	Upregulated
PTS474	ETV5	Tailbud, PSM(S0)	Downregulated (S0 region)
PTS485	MOCH**	somite posterior	No change
PTS542	Nkd2	PSM, somite (dorsal)	No change
PTS635	Calsyntenin-2	PSM(S-1), somite	No change
PTS646	Ets2	PSM (strong at S-1)	Downregulated

EP, expression pattern; WT, wild-type, PSM, presomitic mesoderm; AER, apical ectodermal ridge; NT, neural tube; DM, dermomyotome; *, glucocorticoid induced transcript1; **, mitochondrial oxodicarboxylate carrier homolog; #, GenBank accession number (AB178168).

2. Results

2.1. Screening strategy

Our study has two fundamental aims; to isolate and identify novel genes that are expressed specifically in the PSM and to characterize novel genes that function downstream of Mesp2. To accomplish these goals, we constructed two subtractive cDNA libraries, designated PTS and ST (Fig. 1). The enrichment of specific genes was validated by PCR, using either *G3PDH*- (a ubiquitously expressed gene) or *Mesp2*- (a PSM specific gene) specific primers. *G3PDH* cDNA was found to have been successfully depleted, whereas *Mesp2* cDNA was still evident after repeated subtractions (Fig. 1), suggesting that the subtractive hybridizations had worked effectively. After partial sequencing of randomly selected clones (406 for the PTS and 636 for the ST libraries), an initial search of the GenBank database in NCBI was done using blastn and known genes were removed. As a further screening strategy, we utilized the whole mount ISH technique, using the tail regions of 11.5 dpc embryos. The total number of clones that we subsequently screened by ISH were 251 and 280, for PTS and ST libraries, respectively.

After completion of the ISH screening, we identified more than 30 clones that showed expression in the somite and/or PSM regions. Further sequencing and homology searches using the Celera database identified some of these as regions of known genes (Table 1).

2.2. Characterization of genes obtained by subtractive hybridization

Blastn searches of the GenBank and Celera genome databases identified genes, such as *lymphoid enhancer factor-1* (*LEF1*), that were represented by a number of redundant clones. The clones ST676, PTS566, and PTS629 encode portions of *LEF1* cDNA and ST686, ST762, PTS286, and PTS360 were also identified as intronic sequences of the *LEF1* gene (Table 1 and Fig. 2). During this screening we often obtained intronic DNAs, probably due to the unspliced heterogeneous RNAs since we prepared RNA from whole cells containing nuclei. The intronic DNA fragments sometimes gave rise to different expression patterns, compared with those obtained using exon probes, and these were initially classified differently, as in the case of *LEF1*(Fig. 2) a known nuclear effecter of the Wnt/β-catenin signaling pathway (Porfiri et al., 1997; Hsu et al., 1998). The expression of intronic *LEF1* was observed as an intense band in either S-1 or S-2 of the PSM, in a pattern similar to *Mesp2*, and a lower intensity signal was also observed in the middle PSM. Interestingly the expression was expanded anteriorly in *Mesp2*-null embryos, which is also observed for several genes such as *L-fng* or *Dll1* (Nomura-Kitabayashi et al., 2002). The frequent appearance of this gene, showing these expression patterns, indicated that our strategy could successfully isolate genes that are specifically expressed in the PSM. This was also confirmed for the ST library, from which we isolated two clones, ST313 and ST623, which were identified as *neuropilin-2* and *laminin5*, respectively, and these expression profiles were observed to be confined to the rostral part of somites and are downregulated in Mesp2-null embryos (Table 1 and Fig. 2). Another ST clone, ST371 was identified to be an intronic sequence for *laminin alpha1*, which expression was expanded anteriorly in Mesp2-null embryos (Table 1 and Fig. 2).

Homology searches of the Celera database also determined that clone ST736 contained sequences encoding Axin2 (also named conductin) which functions as a negative regulator of Wnt signaling by inducing β-catenin degradation (Behrens et al., 1998). The expression pattern of

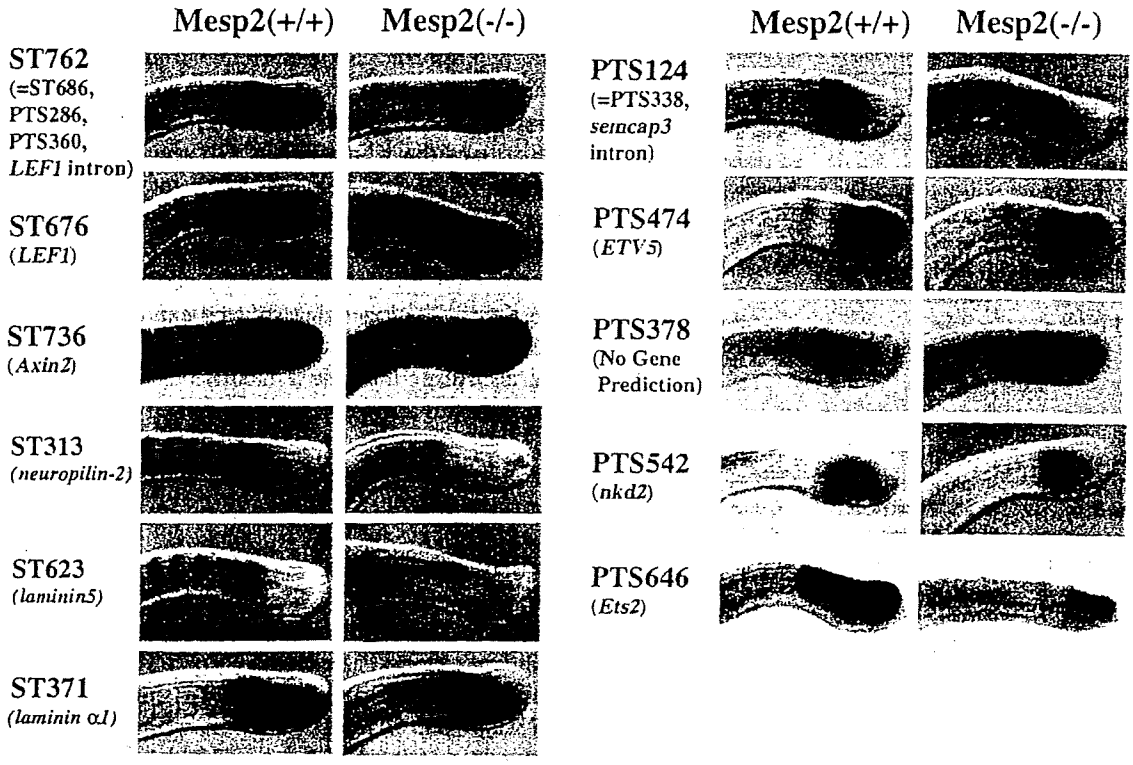

Fig. 2. Expression patterns of cDNA clones selected by ISH screening. ISH were performed with the tail region of wild-type embryos at 11.5 dpc (left side), in comparison to Mesp2-null mutants (right side).

mouse *Axin2* exhibits oscillation in the PSM (Aulehla et al., 2003), with different phase properties from those of *L-fng*, which is an oscillating gene in the Notch signaling pathway. Interestingly, although *Axin2* expression still oscillates when Notch signaling is impaired, a stable stripe of *Axin2* transcripts, in the anterior-most PSM of wild-type embryos, was not observed in Dll1-null mutants (Aulehla et al., 2003). We isolated this clone from our ST library, which may indicate that *Axin2* expression is controlled either directly or indirectly by Mesp2. As shown in Fig. 2, we also observed that the anterior stripe of the *Axin2* transcripts became diffuse and did not form a clear band in Mesp2-null embryos. Celera database searches indicated that the clones PTS124 and PTS338 were intronic sequences of '*M-SEM F cytoplasmic domain-associated protein 3*' (*semcap3*), the expression of which becomes diffuse in the Mesp2-null embryo (Fig. 2). A *Xenopus* homolog of the semcap/GIPC family, kermit, interacts directly with the cytoplasmic portion of the Wnt receptor, frizzled, via its PDZ domain and modulates its signaling activity (Rasmussen et al., 2001; Tan et al., 2001). However, semcap3 has low homology with other family members, and no function has so far been postulated for this protein. PTS474 was identified as '*Ets variant gene 5 (ETV5)*', encoding a transcription factor that contains an Ets DNA binding domain. *ETV5* is expressed in both the tailbud and middle PSM, but not in the anterior-most PSM, and this expression subsequently reappears at the segmental border (Fig. 2). In the Mesp2-null embryo, however, the anterior expression of *ETV5* becomes indistinct. Recently, it has been reported that mouse *ETV5* is expressed in the epithelium of the developing lung and plays a role in epithelial–mesenchymal interactions during lung organogenesis (Liu et al., 2003), but its function in the PSM is still unknown. PTS642 was identified to encode Ets2, another Ets-transcription factor and the expression is downregulated in Mesp2-null embryo (Fig. 2). The expression pattern during morphogenesis has been described (Ristevski et al., 2002). Targeted mutation of Ets2 is reported to result in embryonic lethal before 8.5 dpc due to the defective trophoblast function. However, rescued mice by aggregation with tetraploid embryos are viable and no defect in somitogenesis is reported (Yamamoto et al., 1998). Using either Celera or GenBank database searches, there was no homology detected between PTS378 and known genes. In addition, this clone is unique as it is up-regulated in the absence of Mesp2 (Fig. 2), which was a rare finding during our subtraction analyses. We speculate that this clone may in fact be a member of the non-coding RNAs.

PTS542 was identified as a gene encoding Naked cuticle 2 (Nkd2), the transcript of which is detected in the middle PSM, and it seems that Mesp2 mutation does not affect the expression pattern of *nkd2*. *Naked cuticle* was first identified as a *Drosophila* segment polarity gene (Zeng et al., 2000) and mutation of this gene in the fly embryo causes similar phenotypes to excess Wg expression, indicating that Naked cuticle functions as an inhibitor of Wg signaling.